



Cite this: *Nanoscale Horiz.*, 2023, 8, 1610

## Microfluidic synthesis of nanomaterials for biomedical applications

Yanjuan Huang,<sup>†ab</sup> Chao Liu,<sup>†ab</sup> Qiang Feng<sup>‡\*</sup> and Jiashu Sun<sup>‡\*</sup>

The field of nanomaterials has progressed dramatically over the past decades with important contributions to the biomedical area. The physicochemical properties of nanomaterials, such as the size and structure, can be controlled through manipulation of mass and heat transfer conditions during synthesis. In particular, microfluidic systems with rapid mixing and precise fluid control are ideal platforms for creating appropriate synthesis conditions. One notable example of microfluidics-based synthesis is the development of lipid nanoparticle (LNP)-based mRNA vaccines with accelerated clinical translation and robust efficacy during the COVID-19 pandemic. In addition to LNPs, microfluidic systems have been adopted for the controlled synthesis of a broad range of nanomaterials. In this review, we introduce the fundamental principles of microfluidic technologies including flow field- and multiple field-based methods for fabricating nanoparticles, and discuss their applications in the biomedical field. We conclude this review by outlining several major challenges and future directions in the implementation of microfluidic synthesis of nanomaterials.

Received 1st June 2023,  
Accepted 5th September 2023

DOI: 10.1039/d3nh00217a

rsc.li/nanoscale-horizons

### 1. Introduction

Nanomaterials with unique physicochemical properties are gaining prominence as next-generation dosage forms for drug

administration. The small size of nanomaterials allows for increased drug loading capacity, prolonged blood circulation time, and improved cellular uptake and tissue penetration.<sup>1,2</sup> The specific nanostructures facilitate tunable drug loading and release, targeted delivery of payloads to disease sites, and improved biological efficacy.<sup>3–5</sup> Developing robust and scalable synthesis methods for nanomaterials is crucial for expanding their biological applications and clinical translation.

Synthesis conditions such as solution mixing are of great significance in determining the physicochemical properties of nanomaterials.<sup>6,7</sup> In a typical bottom-up approach, precursor components assemble into nanoparticles through hydrophobic,

<sup>a</sup> Beijing Engineering Research Center for BioNanotechnology, CAS Key Laboratory of Standardization and Measurement for Nanotechnology, National Center for Nanoscience and Technology, Beijing 100190, China.

E-mail: qiang.feng@utsouthwestern.edu, sunjs@nanoctr.cn

<sup>b</sup> University of Chinese Academy of Sciences, Beijing 100049, China

<sup>†</sup> These authors contributed equally to this work.

<sup>‡</sup> Current address: Department of Pharmacology, Simmons Comprehensive Cancer Center, University of Texas Southwestern Medical Center, Dallas, Texas 75390, USA.



Yanjuan Huang

Yanjuan Huang obtained her BS at Huazhong University of Science and Technology in 2021. She then became a PhD student at the National Center for Nanoscience and Technology (NCNST) under the supervision of Prof. Jiashu Sun. Her research focuses on microfluidic-synthesized nanoparticles for cancer immunotherapy.



Chao Liu

Chao Liu, obtained his BS at Hebei University of Technology (2010), followed by a PhD (2016) from University of Chinese Academy of Sciences, working on microfluidics. He joined the National Center for Nanoscience and Technology (NCNST) as a postdoctoral researcher in 2016 and was promoted to Professor in 2020. His research interests include microfluidic separation and detection of rare cells and extracellular vesicles.

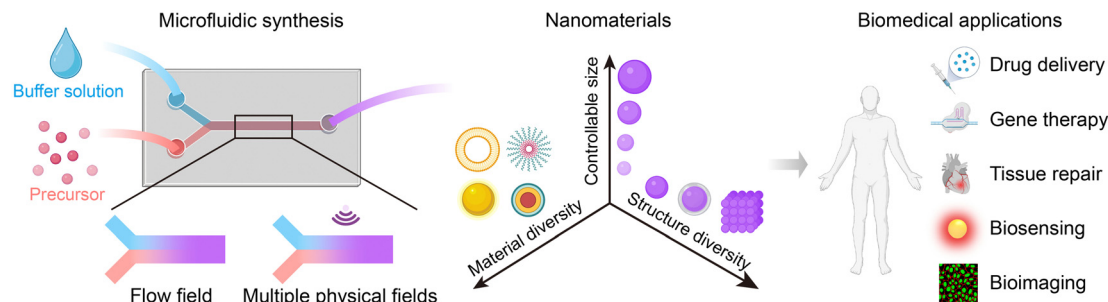


Fig. 1 Overview of microfluidic synthesis of nanomaterials.

electrostatic or coordinate covalent bonding interactions. The same interaction between those components could result in the formation of nanoparticles of different sizes and structures depending on the mixing process.<sup>8–11</sup> Precise control over synthesis conditions is thus required for the reproducible production of nanoparticles, which is also critical for scaling up nanoparticle synthesis.<sup>12,13</sup>

A microfluidic method with accurate manipulation of mass and heat transfer in a confined space holds the potential to advance the field of nanomaterial synthesis. For instance, hydrodynamic mixing in microfluidic channels occurs at the picoliter to microliter scale in a highly controllable, intensive, and uniform manner.<sup>14–21</sup> The multi-stage design of microfluidic systems facilitates the integration of different reactions at predetermined stages, allowing for sequential assembly of complex nanostructures.<sup>22</sup> The coupling of external physical fields with microfluidic systems further improves their capacity to synthesize nanoparticles with functionality diversity.<sup>23–27</sup> Furthermore, high-throughput microfluidic synthesis can be readily achieved through either the continuous flow-based reaction in a single device or using parallel microchannels without the need for re-optimization of synthesis conditions.<sup>28,29</sup> Due to these unique features, microfluidic technologies for nanomaterial synthesis have exponentially grown in recent years.

One of the most successful examples of microfluidics-enabled nanomaterials is the lipid nanoparticle (LNP)-based mRNA vaccines developed during the COVID-19 pandemic.<sup>30</sup>

Using microfluidic platforms for rapid formulation screening and scaling up,<sup>30,31</sup> the first vaccine dose was administered to human patients in a phase I clinical trial within 2 months after obtaining the SARS-CoV-2 whole genome sequence. Taking into account the time required for the preclinical safety and efficacy evaluations, the formulation of vaccines took approximately one month. In phase III clinical trials, the efficacy rate for mRNA-1273 vaccines was 94.5% as reported by Moderna and that of BNT162b2 by Pfizer/BioNTech was 95%.<sup>32</sup> These impressive results can be partially attributed to the use of LNPs as a unique delivery nanocarrier, while the microfluidic platforms played a pivotal role in the successful clinical translation of the LNP-based mRNA vaccines.<sup>31,33,34</sup>

As microfluidic technologies offer a significant advancement in the field of nanomaterials, this review aims to provide an overview of the fundamentals of microfluidic reactors. We summarize the use of microfluidic devices for fabricating various nanomaterials and their applications in the biomedical field (Fig. 1). Additionally, we will discuss the limitations and challenges of microfluidic synthesis, as well as exploring directions for future research.

## 2. Fundamentals of microfluidic reactors

Microfluidic reactors enable precise fluid control and integration of external physical fields, offering highly controllable



Qiang Feng

Qiang Feng obtained his BS (2012) and MS (2014) degrees from Peking University Health Science Center, and he completed his PhD at the National Center for Nanoscience and Technology (NCNST) in 2017. Currently, he is a post-doctoral researcher at the University of Texas Southwestern Medical Center. His research focuses on microfluidics-based nanotechnology for cancer therapy and diagnosis.



Jiashu Sun

Jiashu Sun, received her BSc degree from Beijing Institute of Technology in 2006, and her PhD degree at Vanderbilt University in 2010. She joined the National Center for Nanoscience and Technology (NCNST) as an Assistant Professor in 2011 and has been a Professor/Principal Investigator since 2016. Her current research focuses on the implementation of nanomaterials and microfluidic techniques for bioanalytical chemistry.

synthesis conditions for producing diverse nanomaterials. In this section, we will introduce the advantages of microfluidic synthesis conditions, and present the fundamental methodologies including flow field-based microfluidic reactors and multiple physical field-based microfluidic reactors.

### 2.1 Advantages of microfluidic synthesis conditions

Microfluidic synthesis is typically performed in a bottom-up manner by which precursor components assemble into nanoparticles *via* the management of synthesis conditions such as solvent to anti-solvent (hydrophobicity), ion pair formation (charge-charge) or hydrophobic chelation (coordinate covalent bond).<sup>35,36</sup> Efficient mixing of different reagents in microchannels is crucial for nanoparticle nucleation and growth, which determines the physicochemical properties of nanoparticles. In a typical nanoprecipitation process, the mixing time should be shorter than that for particle nucleation to ensure the formation of monodispersed nanoparticles, while the size of nanoparticles can be tuned by varying the mixing time.<sup>37–39</sup> Although conventional bulk synthesis methods have been widely adopted for synthesizing various nanoparticles, the use of stirrer bars or shakers may result in low efficiency, heterogeneous mixing with large batch-to-batch variation.<sup>40,41</sup> Changes in reaction volumes also have a considerable impact on the bulk mixing, hindering the large-scale production of nanoparticles. In comparison, sufficient mixing in milliseconds can be achieved in microchannels due to the effective mass transfer in small space, which is several orders of magnitude faster than bulk mixing. Moreover, microfluidic synthesis can be feasibly scaled up by parallelizing microchannels without changing the reaction volume in each channel.<sup>42,43</sup> Additionally, the capacity of microfluidic systems can be feasibly expanded by designing sequential multistep synthesis or coupling with physical fields (acoustic, thermal, optical, *etc.*). These integrated microfluidic devices have been utilized to synthesize sophisticated nanoparticles with complex structure and enhanced functionality.

Microfluidics-synthesized NPs with controlled sizes and structures may have better biological outcomes. For example, monodispersed, small, and size-tunable NPs (15–100 nm in diameter) prepared using microfluidic reactors show enhanced biomedical properties and therapeutic effects due to their

effective biological barrier penetration,<sup>44</sup> reduced liver/spleen clearance,<sup>45</sup> enhanced cellular uptake,<sup>46</sup> and passive targeting to tumor sites through the permeability and retention (EPR) effect.<sup>47,48</sup> In addition, NPs with complex structures, such as core-shell NPs, fabricated by the integrated microfluidic devices can improve the drug loading capacity and sustainable release of drugs.<sup>49–51</sup> These core-shell NPs under the camouflage of biological membranes exhibit enhanced immune evasion, prolonged half-life, and better tissue or lesion targeting capabilities.<sup>26,52–54</sup>

### 2.2 Flow field-based microfluidic reactors

The mixing in microfluidic reactors is closely related to the structure of channels and flow rate of fluids in the channels (Table 1). In a microfluidic reactor with the straight microchannel, the flow field is laminar and uniaxial due to the relatively low Reynolds number ( $Re = UW/\nu$ , where  $U$  is the flow speed,  $W$  is the microchannel cross-section dimension, and  $\nu$  is the fluid dynamic viscosity). The resulting diffusive mixing in microchannels is uniform, reproducible but relatively slow, as described by the large Peclet number ( $Pe = Ul/D$ ,  $l$  is the cross-sectional dimension, and  $D$  is the molecular diffusivity), long mixing distance ( $\Delta y_m \sim Pe \times l$ ,  $> 1$  cm), and long mixing time ( $10^2$ – $10^3$  ms).<sup>55</sup> Increasing the concentration gradient is a practical solution for resolving the slow mixing by increasing the diffusion rate. For instance, in hydrodynamic flow focusing (HFF), precursor fluid is squeezed into a narrow middle stream by sheath fluid at large sheath-to-middle flow rate ratios (FRR, usually  $> 10$ ), generating sharp concentration gradients for rapid mixing ( $10$ – $10^2$  ms depending on FRR) (Fig. 2A).<sup>51,56</sup> Although the introduction of sheath fluid effectively shortens the mixing time, a high FRR can also lead to a concentration decrease of nanoparticles, hampering the production yield of HFF.<sup>57,58</sup>

To achieve sufficient and rapid mixing without significant particle dilution, the rational design of microstructures (herring bones, obstacles, *etc.*) or curved microchannel geometries (spiral, serpentine, *etc.*) has been attempted. Microchannels with staggered herringbone structures can enhance the fluid mixing through the generation of transverse microvortices (Fig. 2B).<sup>55,59</sup> The mixing length  $\Delta r$ , over which transverse diffusion homogenizes the solution, is exponentially decreased

**Table 1** Summary of the design and flow conditions of mixing-based microfluidic reactors

Microfluidic reactors	Mixing time	Dimensions of microchannels	Flow conditions	Ref.
Hydrodynamic flow focusing (HFF)	0.04–0.4 ms	Width = 20 $\mu\text{m}$ ; height = 60 $\mu\text{m}$ ; length = 1 cm	Total flow rate = 10.3–11 $\mu\text{L min}^{-1}$	51
Staggered herringbone mixer (SHM)	3 ms 5 ms 5 ms 8 ms	Width = 200 $\mu\text{m}$ ; height = 79 $\mu\text{m}$ Width = 300 $\mu\text{m}$ ; height = 130 $\mu\text{m}$	Total flow rate = 2 $\text{mL min}^{-1}$ Total flow rate = 1.4 $\text{mL min}^{-1}$ Total flow rate = 5 $\text{mL min}^{-1}$ Total flow rate = 3.5 $\text{mL min}^{-1}$	59
Tesla mixer	10 ms	Width = 0.2 mm; depth = 0.2 mm; total length = 4.47 mm	Total flow rate = 10 $\text{mL min}^{-1}$	61
3D double spiral channels	5.51 ms	Width = 300 $\mu\text{m}$ ; height = 300 $\mu\text{m}$ ; length = 6 cm	Total flow rate = 41.25 $\text{mL h}^{-1}$ ; $Re = 60$	64
Flat double spiral microchannels	0.3 ms	Width = 300 $\mu\text{m}$ ; height = 50 $\mu\text{m}$ ; length = 6 cm	Total flow rate = 410 $\text{mL h}^{-1}$ ; $Re = 650$	65

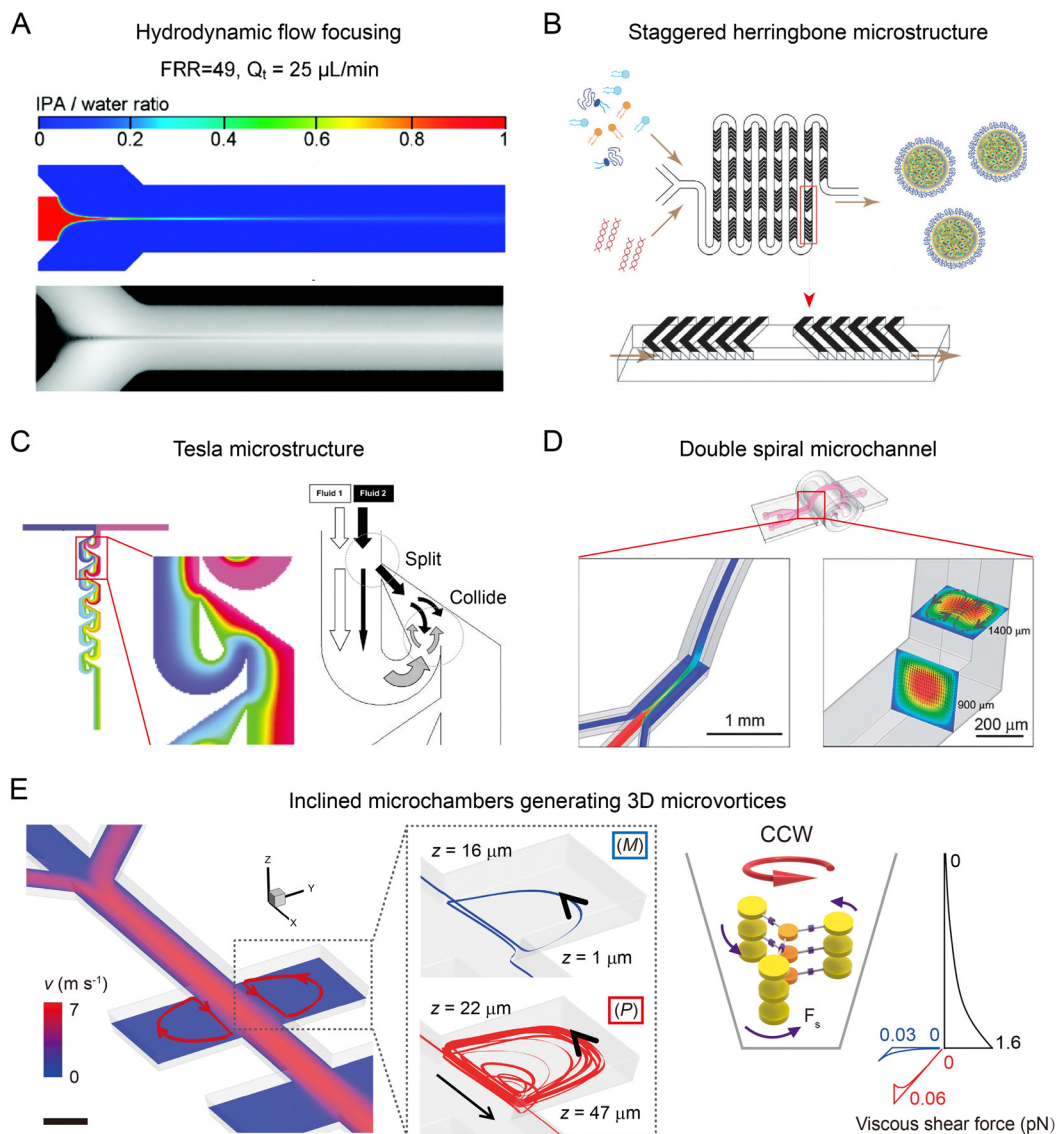


**Fig. 2** Flow field-based microfluidic reactors. (A) Diffusion-based mixing in an HFF-based microfluidic device. Reproduced from ref. 56 with permission from American Chemical Society, Copyright 2010. (B) Chaotic flow induced by staggered herringbone microstructures for enhanced mixing. Reproduced from ref. 59 with permission from American Society of Gene & Cell Therapy, Copyright 2012. (C) Tesla mixer composed of an array of airfoil-shaped obstacles for rapid mixing. Reproduced from ref. 60 with permission from Royal Society of Chemistry, Copyright 2004. (D) Secondary flow generated in a curved microchannel for improved mixing. Reproduced from ref. 64 with permission from Royal Society of Chemistry, Copyright 2013. (E) Inclined microchambers for generating three-dimensional microvortices to induce large shear forces. Reproduced from ref. 23 with permission from Nature Publishing Group, Copyright 2018.

with channel length  $L$ :  $\Delta r \propto W \exp(-L/\lambda)$ , where  $\lambda$  is a characteristic length associated with the trajectories of chaotic flow. Using the staggered herringbones with periodically alternating orientations, the mixing can be accomplished in shorter  $L$  ( $\ln(\text{Pe})W$ ) within  $\sim 10$  ms. Tesla mixer is another powerful tool for effective mixing, in which an array of airfoil-shaped obstacles is placed asymmetrically within the microchannel (Fig. 2C).<sup>60</sup> Fluid near the curved side of an obstacle tends to follow the curved surface and eventually collides with the fluid at the straight side. In this manner, a Tesla mixer can produce transverse dispersion to enhance the mixing with a short mixing time ( $\sim 10$  ms).<sup>61</sup> A bifurcating mixer with

ring-shaped obstacles also achieves effective mixing using a fluid split and merge approach. The microfluidic device composed of a series of bifurcating mixers has been commercialized for the industrial-scale production of lipid- and polymer-based delivery nanoparticles.<sup>62</sup>

Inducing secondary flow such as Dean flow in curved microchannels is another strategy to improve the mixing. The averaged flow speed of Dean flow ( $U_{\text{Dean}}$ ) is described as:<sup>63</sup>

$$U_{\text{Dean}} = \text{Re}^2 \nu / 2R \quad (1)$$

where  $R$  is the radius of curvature of the microchannel. The strong dependence of  $U_{\text{Dean}}$  on  $\text{Re}$  ( $\text{Re}^2$ ) indicates that effective

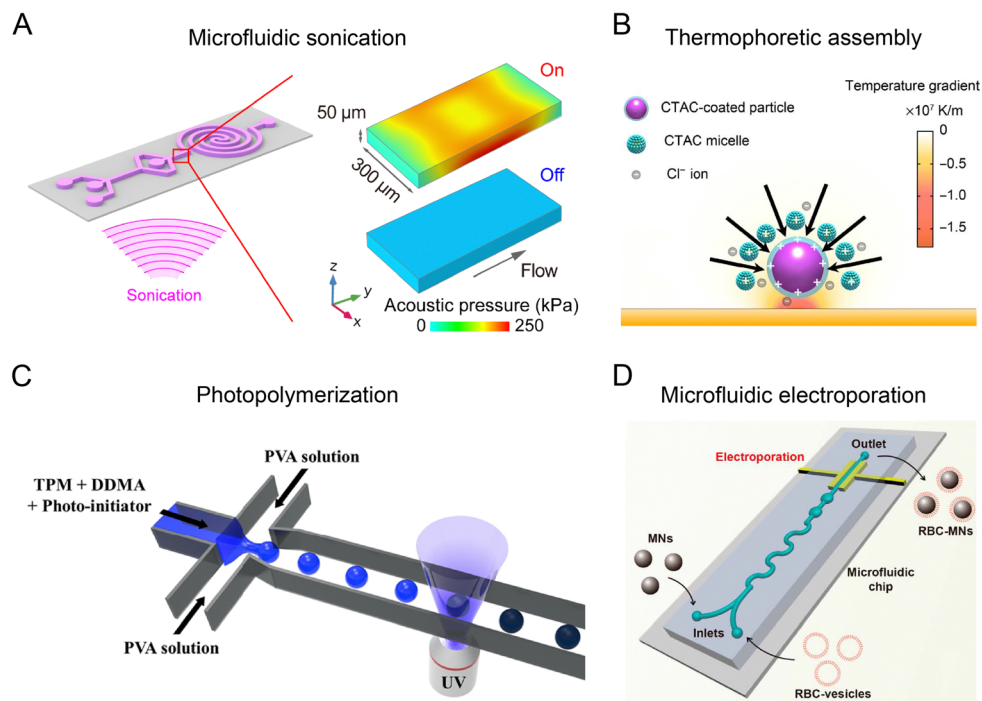


**Fig. 3** Microfluidic reactors integrated with external physical fields. (A) Microfluidic platform integrated with an acoustic field. Reproduced from ref. 26 with permission from American Chemical Society, Copyright 2019. (B) Microfluidic platform combined with thermophoretic nanoparticle manipulation upon localized laser heating. Reproduced from ref. 83 with permission from American Association for the Advancement of Science, Copyright 2017. (C) Microfluidic reactor combined with optical field. Reproduced from ref. 81 with permission from Nature Publishing Group, Copyright 2018. (D) Microfluidic platform integrated with electroporation. Reproduced from ref. 27 from American Chemical Society, Copyright 2017.

mixing can be attained at high flow rates. As an example, the microfluidic reactor with a double-spiral mixing section has a short mixing time down to 6 ms at Re of 60 (Fig. 2D).<sup>64</sup> Further increasing the Re to 650 using a high flow rate of 410 mL h<sup>-1</sup> can reduce the mixing time to 0.3 ms.<sup>65</sup> In a planar microchannel with sudden expansion or contraction, symmetric microvortices arising from the abrupt velocity change can promote the mixing at Re of 30–150.<sup>66</sup> A similar approach has been implemented in coaxial capillary systems, where toroidal microvortices are generated at the intersection of inner and outer capillaries with mismatched injecting flow speeds. This capillary system allowed the nanoparticle synthesis at a flow rate of > 500 mL h<sup>-1</sup> with Re up to 1300.<sup>41</sup>

Apart from enhanced mixing in microfluidic reactors, exploration of hydrodynamic forces in microchannels has been attempted for controlled synthesis of nanomaterials. Microfluidic reactors with small dimensions ( $W$ ) can induce large shear rates (scale as  $U/W$ ) or shear rate gradients ( $U/W^2$ ). In a pair of inclined microchambers, counter-clockwise/clockwise (CCW/CW) vortices with predominantly  $P/M$  chirality are generated due to their tendency of spiraling upward (Fig. 2E).<sup>23</sup> These chiral vortices with high shear rate gradients up to  $8 \times 10^{10} \text{ m}^{-1} \text{ s}^{-1}$  can induce large shear forces of pN level that compete with intermolecular interactions to control the chirality of nanoscale supramolecular assemblies.

In addition to continuous-flow microfluidic reactors, segmented-flow microfluidic devices are also widely employed

for nanoparticle synthesis which involves the segregation of reactants into individual microdroplets. The advantages of segmented-flow synthesis include homogenous synthesis conditions, compatibility to extreme synthesis conditions, and resistance to reactor fouling,<sup>67,68</sup> enabling the production of high-quality nanoparticles from a wide range of material types.<sup>69–72</sup> Several in-depth review papers are available on segmented-flow microfluidic synthesis.<sup>73–75</sup>

### 2.3 Multiple physical field-based microfluidic reactors

The coupling of flow field with other physical fields, such as acoustic, thermal, optical, electric, and magnetic fields, can further improve the performance of microfluidic reactors to produce nanoparticles with higher uniformity and complexity. For example, the acoustic field generated by piezoelectric transducers or bulk acoustic resonators exerts an extra mechanical force in microfluidic reactors, facilitating the deformation, rupture, and re-assembly of nanoparticles for different synthesis scenarios (Fig. 3A).<sup>26,76,77</sup> Thermal field can be precisely controlled in microchannels due to an efficient heat transfer at small scales, allowing for the synthesis for various types of nanoparticles.<sup>78,79</sup> An interesting example is the use of laser irradiation to produce high temperature gradients ( $10^5$ – $10^7 \text{ K m}^{-1}$ ) in microfluidic channels, which enable the optothermal manipulation of nanoparticle building blocks to assemble into sophisticated nanomaterials (Fig. 3B). An optical field has been employed to control the photoreaction-based

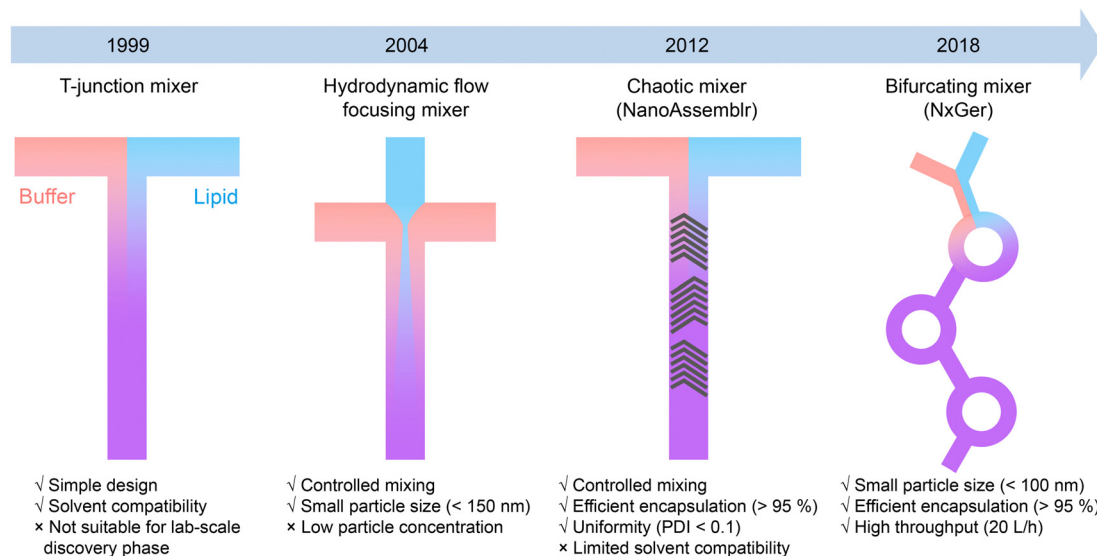


Fig. 4 Evolution of microfluidic reactors for the formulation of RNA/DNA-loaded LNPs.

nanoparticle formation in microfluidic reactors (Fig. 3C).<sup>80,81</sup> Optical microfluidic polymerization can be seamlessly integrated with droplet formation, flow field regulation, or patterned illumination for the synthesis of biocompatible nanoparticles. Leveraging the small length scale, microfluidic reactors can generate intense electric fields (up to  $10^3$  kV m<sup>-1</sup>) to induce effective electroporation for coating biological membrane onto the nanoparticles (Fig. 3D).<sup>27,82</sup> A magnetic field can be used to trap and release magnetic precursors or nanoparticles with precise positioning and timing, allowing for the controlled synthesis and post-processing of magnetic nanoparticles. Therefore, the integration of multiple fields expands the range of nanomaterials that can be synthesized in microfluidic reactors, opening up new avenues for drug delivery and other biomedical applications.

### 3. How microfluidic platform benefits LNP mRNA vaccine

The development of LNP-based mRNA vaccines has been a remarkable achievement in the field of nanomedicine.<sup>84</sup> The first demonstration of LNPs ability to deliver exogenous mRNA to host cells was reported in 1978.<sup>85,86</sup> After that, the cationic lipid- and ionizable cationic lipid-based LNPs were developed for significant improvement of the loading efficiency and transfection efficiency of genetic drugs.<sup>87,88</sup> Notably, the physicochemical properties of LNPs, such as size, dispersity, and zeta potential, dramatically affect the biodistribution and therapeutic effects. However, early attempts to fabricate LNPs suffered from issues such as large particle sizes, large batch-to-batch variation, and difficulty in mass production, making LNPs unsuitable for clinical use.<sup>89–91</sup>

To address those challenges, microfluidic technologies are employed to control the synthesis process. Generally, lipids (including cationic lipids, helper lipids, PEG-lipids, *etc.*)

dissolved in an organic solvent are rapidly mixed with an aqueous buffer solution in the microfluidic reactor to form monodispersed LNPs.<sup>30,84</sup> As shown in Fig. 4, the first microfluidic device used for LNP synthesis was a T-junction based mixer, which was able to produce plasmid DNA-loaded LNPs with diameters of 100–150 nm.<sup>92</sup> Later, Apolipoprotein B (ApoB)-targeting siRNA loaded LNPs (diameters of 77–83 nm, polydispersity index (PDI) of 0.09–0.15) were successfully synthesized by the T-junction microfluidic mixer, representing one of the earliest LNPs used in clinical study.<sup>93</sup> Other microfluidic mixing strategies, including HFF<sup>56,94</sup> and staggered herringbone mixer (SHM),<sup>59,95</sup> enabled the production of LNPs at small sample volumes. These methods were employed for high-throughput screening of up to 70 lipid-like materials for the formulation of RNA-loaded LNPs with tunable diameters of 20–150 nm and PDI down to 0.02. Microfluidics-synthesized LNPs not only exhibit better morphology and reproducibility than traditional lipoplex but also demonstrate improved efficacy. The microfluidic systems, such as SHM-based chaotic mixer (also termed as NanoAssemblr) and bifurcating mixer (NxGen), thus become promising tools for the production of LNP-based mRNA vaccines or LNPs encapsulated with siRNAs<sup>96,97</sup> and sgRNAs/Cas9-mRNA.<sup>98,99</sup> These microfluidic technologies ensure the robust efficacy and rapid translation of LNP-based gene therapy from lab-scale discoveries to commercial-scale production.

### 4. Flow field-based microfluidic synthesis of nanomaterials

The flow field-based microfluidic reactors with rapid mixing are not only suitable for the synthesis of LNPs, but also allow robust generation of a broad range of other nanomaterials. In this section, we introduce the synthesis of nanomaterials with

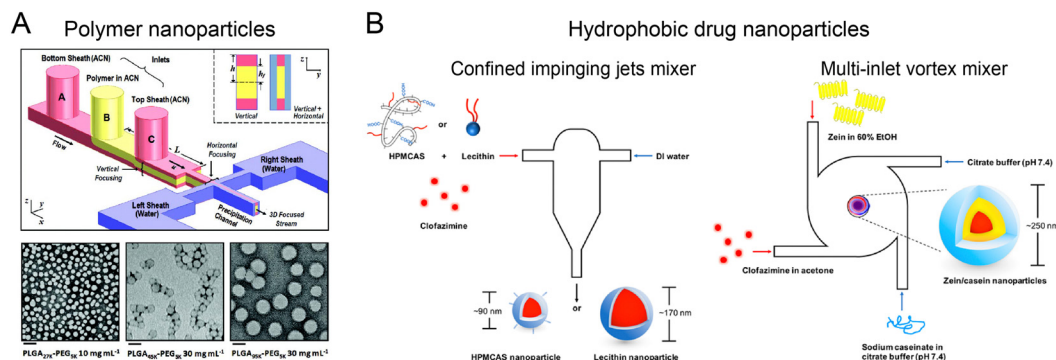


Fig. 5 Mixing-based nanoprecipitation in microfluidic reactors. (A) PLGA nanoparticles fabricated by a 3D HFF-based microfluidic reactor. Reproduced from ref. 100 with permission from Wiley-VCH, Copyright 2011. (B) Hydrophobic drug-loaded nanoparticles by FNP in CIJM and MIVM. Reproduced from ref. 115 with permission from American Chemical Society, Copyright 2017.

controllable sizes and structures by the flow field-based microfluidic reactors.

#### 4.1 Mixing-based nanoprecipitation in microfluidic reactors

Nanoprecipitation is a simple yet effective approach to generate nanomaterials (*e.g.*, polymers and hydrophobic drugs) through the local supersaturation when solvent is mixed with anti-solvent. The synthesis of size tunable nanoparticles with small PDI can be achieved by controlling the mixing time in microfluidic reactors to be shorter than the formation time of nanoparticles.

HFF is one of the prevalent strategies for producing polymer nanoparticles through mixing-based nanoprecipitation.<sup>51,100,101</sup> Typically, a water-miscible organic solvent containing polymer and cargos is flanked by two aqueous anti-solvent streams. Supersaturation induced by rapid mixing drives the polymer precursor to assemble into nanoparticles. Among numerous polymer species, poly(lactic-*co*-glycolic acid) (PLGA) has been approved by FDA for drug formulation.<sup>102</sup> To produce PLGA nanoparticles, a 2-stage HFF microfluidic reactor was used for 3D focusing of polymer solution, which improved the nanoprecipitation process by reducing the channel fouling (Fig. 5A).<sup>100</sup> This method allowed for size-tunable (30–200 nm) production of PLGA-PEG nanoparticles by adjusting the polymer molecular weight ( $M_w$ ) and concentration. By using a double spiral microchannel for HFF, vigorous mixing between an organic solution of PLGA and PEG-*b*-PDPA and water was realized within <1 ms at a high flow rate (243 mL h<sup>-1</sup>) to fabricate small (50 nm), rigid (1.4 GPa), and pH-sensitive nanocomplexes (RPNs).<sup>103</sup> The RPNs exhibited enhanced cellular uptake and lysosome escape, showing higher therapeutic efficacy in a Dox-resistant cancer model. To date, HFF-based nanoprecipitation has been demonstrated for the effective synthesis of PLGA nanoparticles loaded with various drugs, including lipophilic,<sup>104,105</sup> amphiphilic<sup>106,107</sup> or a combination of hydrophilic and hydrophobic drugs.<sup>108</sup> Other biopolymer nanoparticles, including chitosan,<sup>46,109,110</sup> hyaluronic acid,<sup>111</sup> heparin,<sup>112</sup> alginate,<sup>113</sup> and shellac,<sup>114</sup> have also been synthesized for enhanced drug-conjugation efficiency, improved cellular uptake, and reduced cytotoxicity.

Flash nanoprecipitation (FNP) is another method for generating highly loaded nanoparticles by using copolymer stabilization, which can be implemented in microfluidic reactors, such as confined impinging jets mixer (CIJM) and multi-inlet vortex mixer (MIVM). By controlling the timescales of nucleation, aggregation, and stabilization, nanoparticles with precise size, structure, and therapeutic load can be fabricated.<sup>57</sup> For example, CIJM and MIVM were used to prepare clofazimine nanoparticles using various stabilizers (Fig. 5B).<sup>115</sup> In this method, organic solutions of hydrophobic clofazimine and amphiphilic stabilizer (hypromellose acetate succinate, lecithin, or Zein protein) and anti-solvent solutions were injected from different inlets into a microchamber at high velocity. The strong collision of different solutions led to a rapid mixing, resulting in the high supersaturation level for the formation of small, uniform clofazimine nanoparticles (90–250 nm, PDI of 0.11–0.24 depending on stabilizer type). These nanoparticles exhibited higher encapsulation efficiency (>90%) and superior dissolution rates in intestinal conditions compared to Lamprene (clofazimine capsules).

Notably, mixing-based microfluidic reactors enable the synthesis of nanoparticles with tailored sizes, architectures, and surface modification for highly targeted biological outcomes. A HFF microfluidic reactor was used to fabricate size-tunable PLGA NPs (40–160 nm) by adjusting flow conditions and concentrations of precursor and stabilizer. The small curcumin-loaded PLGA NPs (less than 100 nm) showed fast mucus penetration and enhanced potential for pulmonary-targeted delivery. In contrast, PLGA NPs fabricated by bulk mixing had a larger size of 145 nm with reduced mucus penetration.<sup>116</sup> Recently, a chaotic-mixing microfluidic reactor was designed to fabricate gold nanoparticles (AuNPs) with reproducible control in their architecture (branched or regular shape). AuNPs of different shapes induced differential stresses at the cell membrane, resulting in architecture-dependent targeting to subcellular locations and biological effects (histone modification and adjuvant-like immune response).<sup>117–119</sup> A HFF microfluidic reactor incorporated with a multichannel premixing step has been utilized for combinatorial synthesis and optimization of polymer nanoparticles. A library of

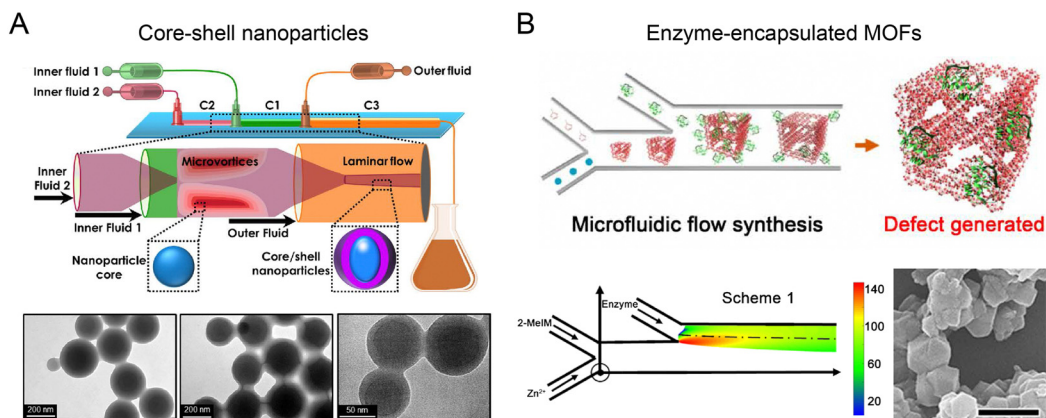


Fig. 6 Sequential assembly of nanomaterials in microfluidic reactors. (A) A two-stage microfluidic nanoprecipitation platform for high throughput production of drug-loaded core-shell nanoparticles. Reproduced from ref. 121 with permission from American Chemical Society, Copyright 2017. (B) A double-Y-shaped microfluidic reactor for the synthesis of enzyme-encapsulated MOF nanoparticles. Reproduced from ref. 127 with permission from American Association for the Advancement of Science, Copyright 2020.

different formulations of PLGA nanoparticles with different sizes, surface PEG coverages, and targeting ligand densities was synthesized and sequentially screened for optimal macrophage uptake evasion and prostate cancer cell targeting. *In vivo* study showed that the cancer-targeted NPs demonstrated a 3.5-fold increase in tumor accumulation compared to non-targeted NPs.<sup>120</sup>

#### 4.2 Sequential assembly of nanomaterials in microfluidic reactors

Nanoparticles with unique, complex structures (*e.g.*, core-shell, multilayer, and porous) facilitate versatile drug loading, improved bio-nano interaction, and better biological outcomes. Multi-stage microfluidic reactors with precise control over the timing and extent of mixing are especially beneficial for sequential assembly of complex nanoparticles.

A two-stage microfluidic reactor containing co-axial capillary HFF was used to fabricate nanoparticles with an enteric polymer shell (Fig. 6A).<sup>121</sup> In the first stage, a mixture of drug (PTX and SFN) and enteric polymer was rapidly mixed with the drug's non-solvent to generate drug cores, followed by mixing with the enteric polymer's non-solvent for the coating of polymer shells in the second stage. By exploiting turbulence-enhanced mixing at  $Re$  up to 1300, core-shell nanoparticles with a diameter of  $\sim 100$  nm and a PDI of  $< 0.1$  were fabricated at a high throughput of  $\sim 700$  g per day. These nanoparticles displayed an ultrahigh drug loading degree (drug mass fraction  $> 40\%$ ) with enhanced payload dissolution kinetics. A three-stage mixing-based microfluidic reactor has been developed for fabricating complex hybrid nanoparticles comprising a hollow water core, a PLGA shell, and an outer lipid layer.<sup>122</sup> In the first stage, an aqueous solution of hydrophilic reagents and two organic solutions of lipids and PLGA were mixed by HFF to generate the reverse micelles. In the second stage, two side water streams were introduced to rapidly precipitate PLGA onto the reverse micelles, resulting in the formation of water core-PLGA shell nanoparticles. Notably, this process is difficult to

control in bulk methods without extensive use of emulsifiers and stabilizers given that reversal micelles are only stable for a very short time.<sup>123</sup> In the third stage, the nanoparticles were coated with another layer of lipids. These hybrid nanoparticles can encapsulate hydrophilic siRNA in the water core and hydrophobic Dox in the PLGA shell, showing a significantly enhanced anti-tumor effect in a multidrug-resistant tumor model.

Highly porous metal-organic frameworks (MOFs) show great promise for therapeutic protein loading and delivery.<sup>124–126</sup> Recently, a double Y-shaped microfluidic reactor with adjustable mixing conditions has been reported to produce enzyme-encapsulated zeolitic imidazolate framework-8 (ZIF-8) nanoparticles (Fig. 6B).<sup>127</sup> Precursors,  $Zn^{2+}$  and 2-methylimidazole (2-MeIM) were injected into the first Y junction at low flow rates ( $\sim mm\ s^{-1}$ ) for the formation of ZIF-8 nanoparticles through Zn-N coordination. The protein cargos such as enzymes were subsequently encapsulated into ZIF-8 nanoparticles at the second Y junction. Because of the laminar and uniaxial flow pattern, the controlled gradient mixing at the fluid interface led to a continuous variation of 2-MeIM/Zn concentration ratio, generating structural defects in MOFs to enhance the access of substrates to the encapsulated enzymes. This reaction condition is difficult to achieve in conventional bulk solution synthesis, due to its insufficient control over spatial and temporal mixing. The microfluidics-generated glucose oxidase (GOx)-loaded MOF demonstrated  $\sim 98\%$  activity of native GOx, an order of magnitude higher than the counterparts produced from bulk synthesis.

#### 4.3 Hydrodynamic force-controlled assembly of nanostructures

Hydrodynamic forces generated from unique flow fields in microfluidic reactors can be used for controlling the assembly of nanomaterials.<sup>128,129</sup> A microfluidic reactor capable of generating a 3D microvortex has been developed to direct the formation of supramolecular assemblies with controlled chirality.<sup>23</sup> Achiral building blocks (TPPS<sub>4</sub> or BTAC) and buffer



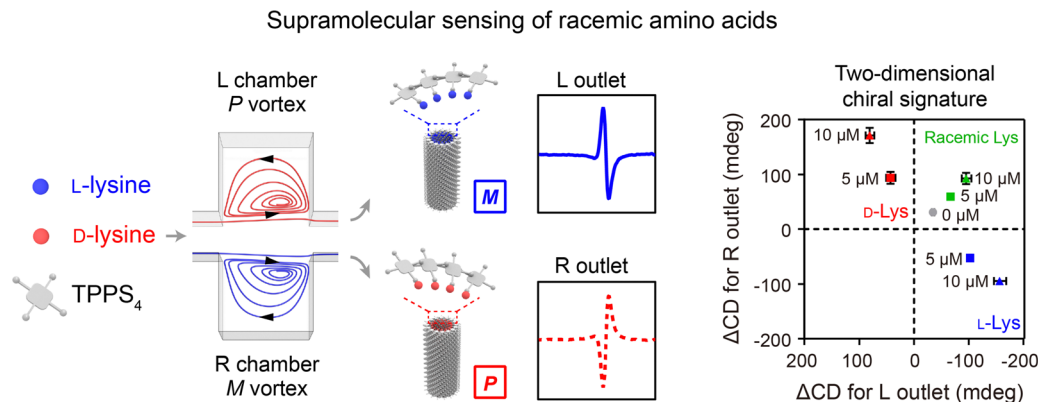


Fig. 7 Hydrodynamic force-controlled assembly of nanostructures. The chiral microvortices exerted high shear forces to control the emerging chirality of the co-assemblies of amino acids and TPPS<sub>4</sub>, allowing for quantitative detection of racemic or enantiomeric amino acids. Reproduced from ref. 130 with permission from Wiley-VCH, Copyright 2020.

solution (acidic buffer or anti-solvent) were injected into an array of inclined microchambers at a high flow velocity ( $7 \text{ m s}^{-1}$ ). The generated 3D microvortices enabled rapid fluid mixing, leading to the formation of supramolecular nuclei through the self-assembly of building blocks. Meanwhile, the microvortices with *P/M* chirality exerted a pN-level shear force to align and twist the supramolecular nuclei, allowing for control over the initial chiral bias within milliseconds. After subsequent growth, supramolecular gels or nanotubes with nearly absolute chirality were obtained. In contrast to laminar chiral microvortices, the flow in stirring cuvettes failed to determine the chirality of nanoassemblies due to turbulent vortices and low shear rate gradients. The chiral microvortices were also used to control the emerging chirality of the co-assemblies of amino acids and TPPS<sub>4</sub>, which served as the template for further assembly of amino acids with compatible chirality (Fig. 7).<sup>130</sup> By detecting the chiral sign and intensity of the supramolecular assemblies collected from different outlets of the microfluidic reactor, quantitative detection of racemic or enantiomeric amino acids was realized.

## 5. Multiple physical field-based microfluidic synthesis of nanomaterials

Incorporating externally applied physical fields, such as acoustic, thermal, optical, electric, and magnetic fields, into microfluidic reactors has become a promising approach for generating nanoparticles with sophisticated structures and enhanced functionalities.

### 5.1 Acoustofluidic synthesis

Acoustofluidics (the combination of acoustics and microfluidics) has been exploited to synthesize nanoparticles in a highly-controllable manner by inducing strong mechanical forces. A notable example is the development of a two-stage acoustofluidic microreactor for fabricating biomimetic core-shell nanoparticles (Fig. 8A).<sup>26</sup> The reactor was immersed into an ultrasonic bath (100 W at 80 kHz) to generate an intense

acoustic field in the microchannels. The first stage was designed for the formation of monodispersed PLGA nanoparticles through organic/aqueous interfacial nanoprecipitation at a high flow rate ( $167 \text{ mL h}^{-1}$ ,  $Re \sim 250$ ). The second stage consisting of a double spiral microchannel enabled efficient rupture of exosome membrane (EM) under an intense acoustic stress ( $10^2 \text{ kPa}$ ), facilitating the reassembly of EM on PLGA nanoparticles to form core-shell nanoparticles within 30 ms. The assembled EM-PLGA nanoparticles (179 nm, PDI 0.22) exhibited superior circulation half-life, reduced monocyte uptake, and improved targeting ability to homologous A549 tumors as compared to lipid-coated PLGA nanoparticles of similar size. The acoustofluidic microreactor has been further adopted in fabricating EM-coated ZIF-8 nanoparticles that were encapsulated with Rhodamine B for precise, *in situ* imaging of cellular ATP.<sup>131</sup> In another study, a T-junction acoustofluidic microreactor has been developed to synthesize eutectic gallium indium (EGaIn) liquid metal nanoparticles (Fig. 8B).<sup>132</sup> The acoustic field provided additional mechanical forces to overcome the strong surface tension of EGaIn liquid metal at the T junction to generate EGaIn microdroplets, which were subsequently broken down into nanodroplets for producing EGaIn nanoparticles functionalized with antibodies. Additionally, by exploiting microstructure vibration and fluid agitating within acoustofluidic microreactors, rapid mixing at the millisecond scale can be achieved for fabricating diverse nanoparticles, including budesonide nanodrugs (80 nm), DNA nanoparticles (63 nm), and BCA-P<sub>114</sub> protein nano-assemblies.<sup>133,134</sup>

### 5.2 Thermal microfluidic synthesis

The introduction of thermal energy into microfluidic reactors can improve mixing efficiency and mass transfer at high temperatures. Thermal microfluidic synthesis has been employed to fabricate a diverse range of nanoparticles, such as biopolymer nanoparticles, metal nanoparticles, metal-oxide nanoparticles, quantum dots (QDs), and perovskite nanocrystals with potential applications for bioimaging, biosensing, and drug delivery.<sup>135–138</sup> A glass-capillary microfluidic platform with

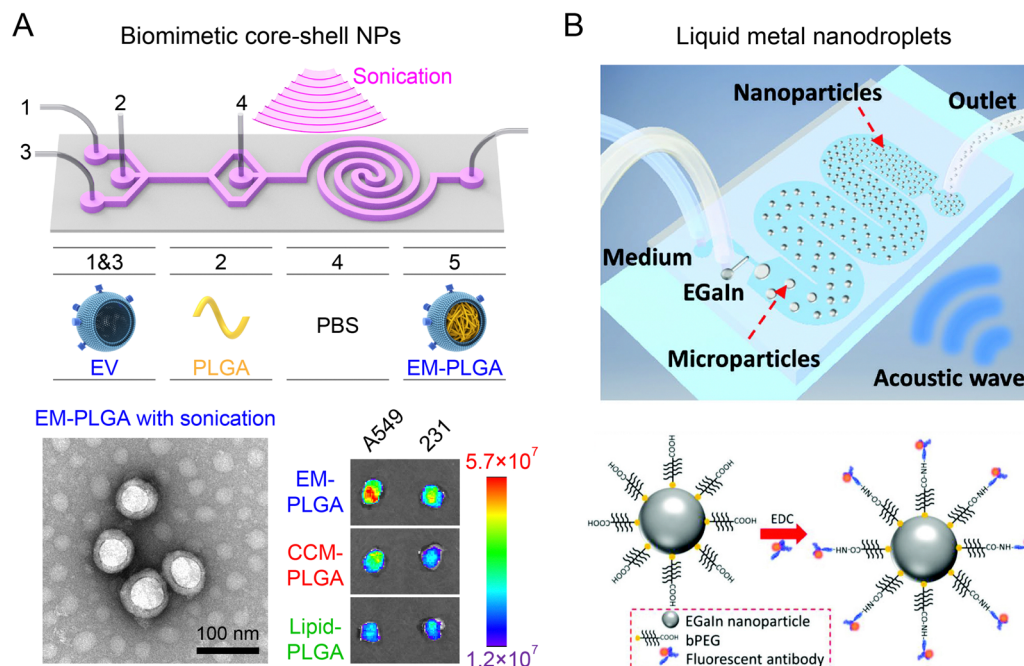


**Fig. 8** Acoustofluidic microreactors for fabricating nanoparticles. (A) A two-stage acoustofluidic microreactor for assembling biomimetic EM-PLGA nanoparticles with improved homotypic tumor targeting. Reproduced from ref. 26 with permission from American Chemical Society, Copyright 2019. (B) An acoustofluidic microreactor for synthesizing EGaIn nanoparticles functionalized with antibodies. Reproduced from ref. 132 with permission from Wiley-VCH, Copyright 2018.

water bath heating was developed for producing  $\beta$ -glucan nanoparticles at a moderate temperature condition (Fig. 9A).<sup>139</sup> Compared to nanoparticles synthesized at room temperature by microfluidics, the  $\beta$ -glucan nanoparticles synthesized at 65 °C had smaller sizes (102 nm) and better colloidal stability. These nanoparticles exhibited better therapeutic efficacy for ameliorating myocardial injury and heart failure than FDA-approved nano-micelles formulation. In

another work, silicon-Pyrex MR-based microfluidic reactors that can tolerate high temperatures (350 °C) and pressures (6 MPa), have been developed for continuous fabrication of metallic nanoparticles.<sup>79</sup> By tuning the temperature and residence time, this method can synthesize an assortment of monometallic (Pt, Au, Pd, *etc.*) and bimetallic (Pt-Ru, Pt-Ni, Pt-Co, *etc.*) nanoparticles with various configurations (nanodumbbells, nanosheets, nanodendrites, *etc.*). Using an oil bath

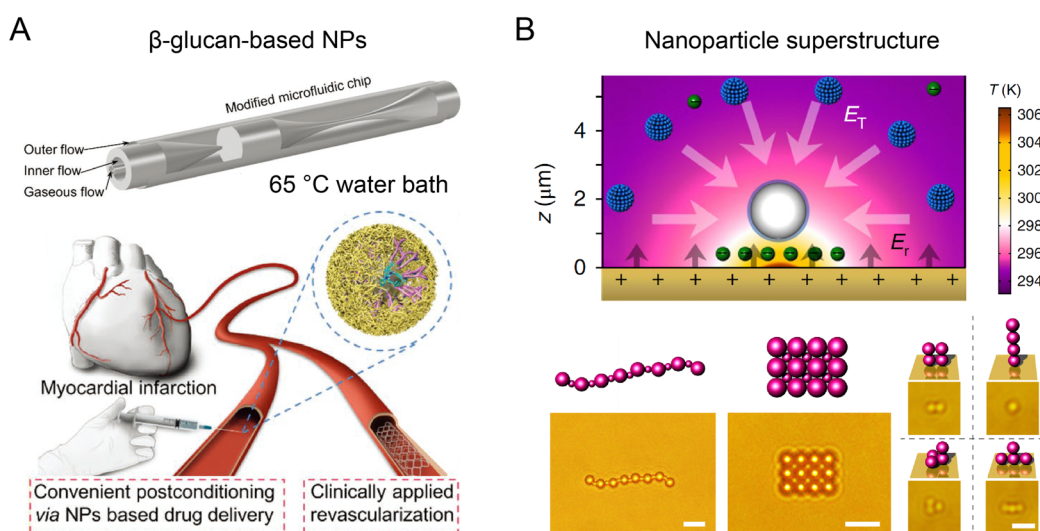


**Fig. 9** Thermal microfluidic reactors for fabricating functional nanoparticles. (A) A glass-capillary microfluidic platform with water bath heating to synthesize  $\beta$ -glucan nanoparticles for cardiac targeting drug delivery. Reproduced from ref. 139 with permission from Wiley-VCH, Copyright 2022. (B) Thermophoretic assembly of nanoparticles into functional superstructures. Scale bars, 5  $\mu$ m (left) and 2  $\mu$ m (right). Reproduced from ref. 83 with permission from American Association for the Advancement of Science, Copyright 2017.

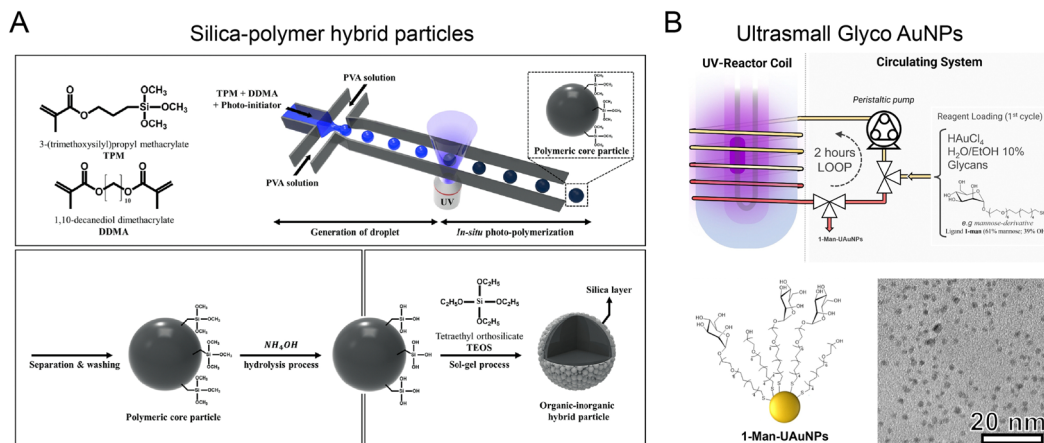


Fig. 10 Optical microfluidic reactors for synthesizing various nanoparticles. (A) An optical microfluidic reactor for fabricating organic–inorganic core–shell particles through UV polymerization. Reproduced from ref. 81 with permission from Nature Publishing Group, Copyright, 2018. (B) Photo-induced microfluidic synthesis of ultrasmall gold nanoparticles engineered with glycans. Reproduced from ref. 154 with permission from Wiley-VCH, Copyright 2022.

(160–200 °C), a thermal microfluidic reactor was reported to fabricate iron@iron-oxide core–shell nanoparticles by thermal decomposition of  $\text{Fe}(\text{CO})_5$  precursor in the presence of surfactant oleylamine.<sup>140</sup> The byproduct of CO gas formed an gas–liquid two-phase system to induce Dean-Taylor vortices for enhanced mixing during synthesis. Moreover, thermal microfluidic reactors integrated with droplet-based precursor encapsulation have been used for the robust synthesis of semiconductor QDs ( $\text{CdSe}$ ,  $\text{Ag}_2\text{S}$ ,  $\text{ZnO}$ ) and perovskite nanocrystals with tunable size and emission spectra.<sup>141–143</sup> The thermal microfluidic reactors with multistage configurations further enabled additional surface modification procedures for the formation of high-performance core–shell QDs ( $\text{ZnSe}/\text{ZnS}$ ,  $\text{CuInS}_2/\text{ZnS}$ ,  $\text{InP}/\text{ZnS}$ , *etc.*).<sup>144,145</sup>

In addition to thermal microfluidic reactors using homogeneous temperature conditions, thermophoresis arising from a

localized heating-induced temperature gradient in the microreactor offers an innovative approach to assemble various nanoparticles into functional superstructures (Fig. 9B).<sup>83,146,147</sup> In a microchamber containing the mixture of nanoparticles and ionic surfactant cetyltrimethylammonium chloride (CTAC), a sharp temperature gradient (up to  $\sim 10^7 \text{ K m}^{-1}$ ) induced by laser heating of the Au substrate resulted in the generation of a localized electric field upon the differentiated thermophoretic depletion of CTAC and  $\text{Cl}^-$ . The negatively-charged CTAC-absorbed nanoparticles were electrophoretically trapped at the hot spot to form nanoparticle assemblies, which were then stabilized upon the inter-particle bonding arising from depletion attraction force, van der Waals interaction, and electrostatic interaction. The thermophoresis technique enabled the fabrication of nanoparticle assemblies of diverse materials (metal, metal oxide, polymer) and configurations (1D chains, 2D patterns, and

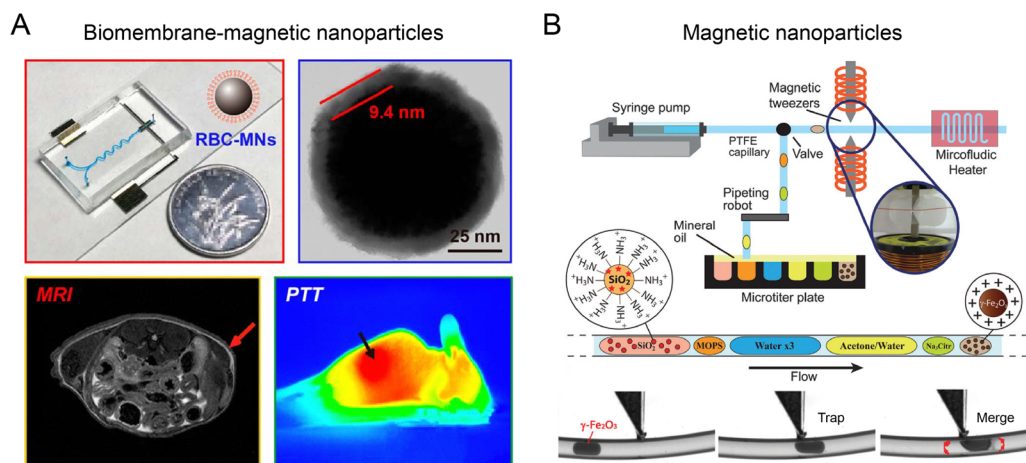


Fig. 11 Electric or magnetic microfluidic reactors for the formation of nanoparticles. (A) A microfluidic reactor consisting of an electroporation zone to fabricate core–shell RBC-MNPs with enhanced MRI and PTT. Reproduced from ref. 27 from American Chemical Society, Copyright 2017. (B) A droplet-based microfluidic reactor coupled with a magnetic tweezer for generating  $\text{SiO}_2@ \gamma\text{-Fe}_2\text{O}_3$  nanoparticles. Reproduced from ref. 157 from Royal Society of Chemistry, Copyright 2015.

Table 2 Characteristics, advantages, disadvantages of each microfluidic technique for producing NPs

Microfluidic reactors	Characteristics and mechanism	Advantages	Disadvantages	Nanoparticle production
Hydrodynamic flow focusing (HFF)	The sheath streams focus the intermediate sample streams in a narrow region, shortening the mixing distance	(1) Easy integration into existing microfluidic devices (2) Rapid and efficient mixing	(1) Low particle concentration (2) Possibility of particle aggregation or sedimentation at the interface between different fluid streams	LNPs, polymeric NPs
Staggered herringbone mixer (SHM)	Employ a pattern of interlocking herringbone grooves on the channel walls to induce chaotic advection and enhance mixing through secondary flows	(1) Efficient and rapid mixing (2) Low sample consumption (3) Scalable production	(1) Complex fabrication process (2) Potential clogging issues due to the presence of grooves (3) Limited solvent compatibility for device materials	LNPs, polymeric NPs
Tesla mixer	One of the fluid streams is split into two streams and then, the two streams combine again to create chaotic advection for enhanced mixing performance	(1) Rapid and efficient mixing (2) Low sample consumption	(1) Low particle concentration (2) Not suitable for low Reynolds number flows	LNPs, polymeric NPs
Microfluidic bifurcating/baffle mixer	Utilize a branching channel structure to divide and recombine fluid streams	(1) Rapid and efficient mixing (2) Low sample consumption (3) Excellent tuning of particle size	Potential uneven distribution of fluids at the recombination point	LNPs, inorganic NPs
Acoustofluidic synthesis	Exert an extra mechanical force in microfluidic reactors, facilitating the deformation, rupture, and re-assembly of nanoparticles for different synthesis scenarios	(1) Improved mixing (2) Reduced particle size (3) Manufacture of biomimetic lipid nanoparticles	(1) Side effect of rapid heating (2) Expensive costs of devices	LNPs, metal NPs, biomimetic membrane-coated NPs
Thermal microfluidic synthesis	Improve heat transfer at small scales	(1) Suitable for the synthesis of thermal-sensitive materials (2) Controlled particle shape because of thermally reversible properties (3) High spatial resolution for colloid assembly	Thermal deformation of the microfluidic channels or materials	Metal NPs, organic NPs, quantum dots
Optical microfluidic synthesis	UV or visible light exposure leads to homogeneous breakage of bonds in the photoinitiator molecules, resulting in the release of free radicals and the formation of bonds between the polymer chains	(1) Trigger the <i>in situ</i> chemical reaction (2) Easy surface functionalization	Potential photochemical or photothermal effects that can influence the reaction	Organic/inorganic hybrid NPs, polymeric NPs
Electric or magnetic microfluidic synthesis	Induce flow instabilities and transversal transport to improve mixing	(1) Allow efficient membrane coating on the surface of nanoparticles (2) Offer a template-free strategy for metal NPs synthesis (3) Control the assembly of nanoparticles	Relatively complex microfluidic device fabrication to implement electric field	LNPs, metal/metal compound NPs, biomimetic membrane-coated NPs

3D structures). These superstructures with unique optical properties hold great potential for biosensing and imaging applications.

### 5.3 Optical microfluidic synthesis

Optical microfluidics offers an effective approach for photo-induced synthesis of nanoparticles. An optical microfluidic platform has been developed to fabricate organic-inorganic core-shell particles through UV polymerization (Fig. 10A).<sup>81</sup> Photocurable droplets containing DDMA (polymer core material) and TPM were generated by flow focusing in the

microchannel. UV irradiation triggered the *in situ* polymerization of DDMA and TPM to form the solid cores. The silane groups exposed on the core surface were further hydrolyzed into activated silanol groups, enabling the attachment of silica nanoseeds for growth into a silica shell in the presence of TEOS. These silica-polymer hybrid particles could serve as versatile delivery platforms for chemotherapeutic agents, antibiotics, MRI contrast agent, *etc.*<sup>148,149</sup> The microfluidic UV polymerization strategy was also applied to fabricate hydrogels from biocompatible polymers, such as hydraulic acid

Table 3 Summary of microfluidic reactors for synthesizing varied nanoparticles and their biomedical application

Microfluidic reactors	Nanoparticles	Main synthesis parameters	Biomedical application	Biological outcomes	Ref.
Two-stage hydrodynamic flow focusing (HFF)	Doxorubicin-loaded PLGA-PEG nanoparticles	Reynolds number (Re) = 133; total flow rate = 243 mL h <sup>-1</sup>	Anti-tumor therapy	Inhibition of tumor growth by 92%	103
Confined impinging jets mixer (CIJM) and multi-inlet vortex mixer (MIVM)	Clofazimine nanoparticles	Flow rate of clofazimine and zein = 12 mL min <sup>-1</sup> ; flow rate of NaCas and citrate buffer = 36 mL min <sup>-1</sup>	Cryptosporidiosis therapy	Improved dissolution characteristic	115
Two-stage microfluidic reactor containing co-axial capillary HFF	Paclitaxel/sorafenib-loaded multilayered core/shell organic nanocomposites	Flow rate of aqueous solution = 4.21 mL min <sup>-1</sup> ; flow rate of paclitaxel or sorafenib drug acetone solution (10 mg mL <sup>-1</sup> ) = 0.42 mL min <sup>-1</sup>	Drug delivery	Ultrahigh drug loading degree and enhanced therapeutic dissolution	121
Three-stage microfluidic reactor	Water core/PLGA shell/lipid layer nanoparticles	Flow rate of hydrophilic molecules = 0.2 mL h <sup>-1</sup> ; flow rate of PLGA and 1,2-dioleoyl-3-trimethylammonium propane = 1 mL h <sup>-1</sup> ; flow rate of water sheaths = 15 mL h <sup>-1</sup>	Anti-tumor therapy in a multidrug-resistant tumor model	Consistent suppression of tumor growth	122
Double Y-shaped microfluidic reactor	Glucose oxidase (GOx)-loaded MOF	Flow rates of zinc nitrate (9.3 mg mL <sup>-1</sup> ), 2-MeIM (102.5 mg mL <sup>-1</sup> ), and enzyme (1 mg mL <sup>-1</sup> ) water solutions = 0.5 $\mu$ L min <sup>-1</sup>	Catalysis, biosensors, and drug delivery	Demonstration of ~98% activity of native GOx	127
Microfluidic reactor capable of generating 3D microvortex	Tetra-(4-sulfonatophenyl) porphyrin (TPPS <sub>4</sub> )-Lys co-assemblies	Flow rate of mixtures of TPPS <sub>4</sub> (20 $\mu$ M) and racemic Lys (5 $\mu$ M) = 30 mL h <sup>-1</sup> ; flow rate of HCl (1.5 M) and C <sub>2</sub> mim <sup>+</sup> (0.4 M) = 1 mL h <sup>-1</sup>	Chiral sensing	NA	130
Two-stage acoustofluidic microreactor	Exosome membrane-coated PLGA nanoparticles	A bath sonicator with a frequency of 80 kHz and a power of 100 W; flow rate of PLGA (5 mg mL <sup>-1</sup> ) and PBS solution = 7 mL h <sup>-1</sup> ; flow rate of exosomes (0.5 mg mL <sup>-1</sup> ) = 80 mL h <sup>-1</sup>	Drug delivery	Enhanced immune evasion and homotypic targeting effect	26
Two-stage acoustofluidic microreactor	Exosome membrane-coated ZIF-8 nanoparticles	A bath ultrasonic instrument with a frequency of 80 kHz and a power of 100 W; flow rate of ZIF-8 loaded with FITC-BSA and PBS solution = 11 mL h <sup>-1</sup> ; flow rate of exosomes (5 $\times$ 10 <sup>10</sup> mL <sup>-1</sup> ) = 80 mL h <sup>-1</sup>	In situ imaging of cellular ATP	Improved immune invasion and enhanced uptake by homotypic tumor cells	131
T-junction acoustofluidic microreactor	Eutectic gallium indium (EGaIn) liquid metal nanoparticles	An ultrasonic transducer with a power of 65 W and a frequency of 20 kHz; flow rate of bPEG = 50 $\mu$ L min <sup>-1</sup> ; flow rate of EGaIn = 1 $\mu$ L min <sup>-1</sup>	Biosensors and photothermal/electric field-induced intracellular delivery	NA	132
Glass-capillary microfluidic platform with water bath heating	$\beta$ -Glucan nanoparticle	Temperature = 65 °C; flow rate of chitosan (0.4 mg mL <sup>-1</sup> ) and phosphorylated barley $\beta$ -1,3-1,4 glucan (0.8 mg mL <sup>-1</sup> ) = 40 mL h <sup>-1</sup> ; flow rate of air = 150 mL h <sup>-1</sup>	Therapy for ameliorating myocardial injury and heart failure	Specific targeting capability toward Dectin-1 <sup>+</sup> macrophage, better therapeutic efficacy than FDA-approved nano-micelles formulation	139
Silicon-Pyrex MR-based microfluidic reactors	Monometallic and bimetallic nanoparticles	Temperature = 25–200 °C; constant back pressure = 0.8–2 MPa; flow rate ratio = 0.5–4	Electronic, optical, and medical applications	NA	79
Thermal microfluidic reactor	Iron@iron-oxide core-shell nanoparticles	Temperature = 180–200 °C; flow rate = 0.05–30 mL min <sup>-1</sup>	Magnetic hyperthermia	NA	140
Microfluidic platform with a light-controlled thermo-electric field	AuNPs with cetyltrimethylammonium chloride (CTAC) micelles	A 532 nm diode-pumped solid-state laser	Biosensing and imaging applications	NA	83
Optical microfluidic platform with UV irradiation	Silica-polymer hybrid particles	Wavelength range of UV light (100 W HBO mercury lamp) = 330–380 nm	Drug delivery and tissue engineering	Highly controlled diffusion of the active compound	81
Optical microfluidic platform	Glycan-decorated ultra-small AuNPs	Flow rate of ligand 1-Man = 0.25 mL min <sup>-1</sup>	Modulation of carbohydrate-mediated recognition events	NA	154
Microfluidic chip with an electro-poration zone	Membrane-coated Fe <sub>3</sub> O <sub>4</sub> magnetic nanoparticles	Pulse frequency = 100 Hz; duration = 200 $\mu$ s; flow velocity = 20 $\mu$ L min <sup>-1</sup> ; voltage = 20–70 V	Tumor magnetic resonance imaging (MRI) and photothermal therapy (PTT)	Better immune escape ability, longer blood circulation, and enhanced MRI and PTT performance	27

Table 3 (continued)

Microfluidic reactors	Nanoparticles	Main synthesis parameters	Biomedical application	Biological outcomes	Ref.
Droplet-based microfluidic reactor coupling of electric fields	Anisotropic gold nanostars	Voltage = 600 V; flow rate of PVP in DMF (37.5 mM) and HAuCl <sub>4</sub> (1.5 mM) = 50 $\mu\text{L h}^{-1}$ ; flow rate of Picosurf-1 = 500 $\mu\text{L h}^{-1}$ ; flow rate of spherical gold seeds of 15 nm = 50 $\mu\text{L h}^{-1}$	Biosensing and bioimaging	NA	70
Droplet-based microfluidic reactor coupling of magnetic fields	Magnetic SiO <sub>2</sub> @ $\gamma$ -Fe <sub>2</sub> O <sub>3</sub> nanoparticles	Magnetic field = 0.3 T; flow rate = 0.02 $\mu\text{L s}^{-1}$	Biomedical diagnosis and nanomedicine	NA	157

derivatives and PEG derivatives, with controllable size, rigidity, and porosities.<sup>150,151</sup> The combination of microfluidic UV polymerization and inertial flow shaping allowed for the production of 3D-shaped particles for biomedical applications including drug delivery and tissue engineering.<sup>152,153</sup> The optical microfluidic reactor was also capable of fabricating glycan-decorated ultrasmall AuNPs (Fig. 10B).<sup>154</sup> Aqueous mixture of HAuCl<sub>4</sub>, thiol-terminated glycan derivatives, and ethanol was infused and circulated into an FEP microtube by a peristaltic pump. UV-induced decomposition of the solvent (water and ethanol) generated hydroxyl radicals and solvated electrons for HAuCl<sub>4</sub> reduction and AuNPs formation. The produced AuNPs functionalized with glycans had a diameter down to  $\sim 6$  nm, with potential applications in modulating carbohydrate-mediated recognition events.<sup>155,156</sup>

#### 5.4 Electric or magnetic microfluidic synthesis

Microfluidic reactors coupled with an electric field have been reported for fabricating biometric nanoparticles in a precise and reproducible manner.<sup>82</sup> A microfluidic reactor consisting of a serpentine microchannel and a downstream electroporation zone ( $\sim 300$  kV m<sup>-1</sup>, pulse duration 0.2 ms) was developed to effectively encapsulate Fe<sub>3</sub>O<sub>4</sub> magnetic nanoparticles (MNPs) into red blood cell (RBC) membrane-derived vesicles (Fig. 11A).<sup>27</sup> Compared to RBC-MNPs fabricated by conventional bulk extrusion, microfluidic electroporation-synthesized RBC-MNPs possessed a more complete cell membrane coating, better colloidal stability, improved immune escape ability, longer blood circulation, and enhanced magnetic resonance imaging (MRI) and photothermal therapy (PTT). The coupling of an electric field with droplet-based microfluidic reactor was used to synthesize anisotropic gold nanostars (AuNSTs).<sup>70</sup> Each droplet containing PVP and gold salt was precisely mixed with an equal volume of Au seeds through electric pico-injection, allowing for the production of AuNSTs of tens of nm with a low batch-to-batch variation.

The integration of magnetic field with a droplet-based microfluidic reactor has been devised for automated, sequential fabrication of magnetic SiO<sub>2</sub>@ $\gamma$ -Fe<sub>2</sub>O<sub>3</sub> nanoparticles (Fig. 11B).<sup>157</sup> A syringe pump combined with a pipetting robot was used to generate deterministic trains of droplets of  $\gamma$ -Fe<sub>2</sub>O<sub>3</sub> precursor suspension, sodium citrate solution, washing buffer, SiO<sub>2</sub> nanoparticle suspension, *etc.* An on-demand trapping of droplets was achieved by applying a magnetic tweezer

across the microchannel for streamlining multistep operations such as mixing, flocculation, redispersion, washing, and surface functionalization. Using this method, monodispersed fluorescent SiO<sub>2</sub>@ $\gamma$ -Fe<sub>2</sub>O<sub>3</sub> nanoparticles (200  $\pm$  4 nm) were synthesized.

## 6. Conclusions and future directions

Microfluidics featuring miniaturization, integration, and high controllability has emerged as a revolutionary technology to accelerate the development of nanomaterials for biomedical applications. Microfluidic reactors, such as flow field-based microfluidic reactors and multiple physical field-based microfluidic reactors, have been demonstrated for synthesizing a diverse range of nanoparticles with complex structure and enhanced functionality in a highly-controllable manner (Table 2). These nanoparticles play an important role in the fields including cancer therapy, imaging, and biosensing (Table 3).

Despite these promising results, further efforts should be directed to improve the development of microfluidic reactors. First, the current maximum mass productivity is limited by the small size of the microchannel which cannot withstand excessive flow rates. To make the transition of microfluidic synthesis from bench to industry, scalable manufacturing of microfluidic devices with parallel reaction arrays and high production rates needs to be considered. Second, the synthesis of three-dimensional complex-structured nanoparticles is not easy even for microfluidic reactors. The adoption of extreme synthesis conditions, such as high temperature, high pressure, and strong acid and alkali, can be attempted in microfluidic reactors for better control of the nanoparticle formation process. Third, although microfluidic synthesis can accelerate the development process of nanomaterials, more efficacy and toxicity testing of those generated nanomaterial need to be conducted in clinical trials in addition to animals. We anticipate that microfluidic technology will become a more versatile and efficient tool for the rapid fabrication, optimization, and translation of nanomaterials.

## Conflicts of interest

There are no conflicts of interest to declare.

## Acknowledgements

This work was supported by the National Natural Science Foundation of China (22025402, 22227805, T2222008, and 22174030), the National Key R&D Program of China (2020YFA0210800 and 2021YFA0909400), The Strategic Priority Research Program of the Chinese Academy of Sciences (XDB36020300), and the CAS Project for Young Scientists in Basic Research (YSBR-036).

## References

- U. Prabhakar, H. Maeda, R. K. Jain, E. M. Sevick-Muraca, W. Zamboni, O. C. Farokhzad, S. T. Barry, A. Gabizon, P. Grodzinski and D. C. Blakey, *Cancer Res.*, 2013, **73**, 2412–2417.
- J. K. Patra, G. Das, L. F. Fraceto, E. V. R. Campos, M. D. P. Rodriguez-Torres, L. S. Acosta-Torres, L. A. Diaz-Torres, R. Grillo, M. K. Swamy, S. Sharma, S. Habtemariam and H.-S. Shin, *J. Nanobiotechnol.*, 2018, **16**, 71.
- M. J. Mitchell, M. M. Billingsley, R. M. Haley, M. E. Wechsler, N. A. Peppas and R. Langer, *Nat. Rev. Drug Discovery*, 2021, **20**, 101–124.
- I. K. Herrmann, M. J. A. Wood and G. Fuhrmann, *Nat. Nanotechnol.*, 2021, **16**, 748–759.
- S. A. Dilliard and D. J. Siegwart, *Nat. Rev. Mater.*, 2023, **8**, 282–300.
- Z. Liu, F. Fontana, A. Python, J. T. Hirvonen and H. A. Santos, *Small*, 2020, **16**, 1904673.
- Y. Zhang, D. Liu, H. Zhang and H. A. Santos, *Microfluidic mixing and devices for preparing nanoparticulate drug delivery systems*, *Microfluidics for Pharmaceutical Applications*, Elsevier, 2019, pp. 155–177.
- H. Xie and J. W. Smith, *J. Nanobiotechnol.*, 2010, **8**, 18.
- S. Hornig, T. Heinze, C. R. Becer and U. S. Schubert, *J. Mater. Chem.*, 2009, **19**, 3838–3840.
- X. Hou, T. Zaks, R. Langer and Y. Dong, *Nat. Rev. Mater.*, 2021, **6**, 1078–1094.
- J. Cravillon, S. Münzer, S.-J. Lohmeier, A. Feldhoff, K. Huber and M. Wiebcke, *Chem. Mater.*, 2009, **21**, 1410–1412.
- M. Šoltys, M. Balouch, O. Kašpar, M. Lhotka, P. Ulbrich, A. Zadrazil, P. Kovačik and F. Stepanek, *Chem. Eng. J.*, 2018, **334**, 1135–1147.
- X. Liu and H. Meng, *View*, 2021, **2**, 20200190.
- S. J. Shepherd, D. Issadore and M. J. Mitchell, *Biomaterials*, 2021, **274**, 120826.
- L.-J. Pan, J.-W. Tu, H.-T. Ma, Y.-J. Yang, Z.-Q. Tian, D.-W. Pang and Z.-L. Zhang, *Lab Chip*, 2018, **18**, 41–56.
- J. Ma, S. M.-Y. Lee, C. Yi and C.-W. Li, *Lab Chip*, 2017, **17**, 209–226.
- Y. Liu, H. Shen, X. Yang, S. Kang, L. Cai, T. Tian, R. Su, C. Yang and Z. Zhu, *Trac, Trends Anal. Chem.*, 2023, **158**, 116894.
- L. Zhang, Q. Chen, Y. Ma and J. Sun, *ACS Appl. Bio Mater.*, 2020, **3**, 107–120.
- J. Chang, Y. Zhang, Y. Li, Z. Han, F. Tian, C. Liu, Q. Feng, Y. Wang, J. Sun and L. Zhang, *Small Methods*, 2021, **5**, 2001047.
- F. Zhu, Y. Ji, J. Deng, L. Li, X. Bai, X. Liu, B. Lin and Y. Lu, *Chin. Chem. Lett.*, 2022, **33**, 2893–2900.
- X. Liu, Q. Yi, Y. Han, Z. Liang, C. Shen, Z. Zhou, J.-L. Sun, Y. Li, W. Du and R. Cao, *Angew. Chem., Int. Ed.*, 2015, **54**, 1846–1850.
- L. Shang, Y. Cheng and Y. Zhao, *Chem. Rev.*, 2017, **117**, 7964–8040.
- J. Sun, Y. Li, F. Yan, C. Liu, Y. Sang, F. Tian, Q. Feng, P. Duan, L. Zhang, X. Shi, B. Ding and M. Liu, *Nat. Commun.*, 2018, **9**, 2599.
- H. Amini, W. Lee and D. Di Carlo, *Lab Chip*, 2014, **14**, 2739–2761.
- M. Yang, Y. Gao, Y. Liu, G. Yang, C.-X. Zhao and K.-J. Wu, *Chem. Eng. Sci.*, 2021, **234**, 116450.
- C. Liu, W. Zhang, Y. Li, J. Chang, F. Tian, F. Zhao, Y. Ma and J. Sun, *Nano Lett.*, 2019, **19**, 7836–7844.
- L. Rao, B. Cai, L.-L. Bu, Q.-Q. Liao, S.-S. Guo, X.-Z. Zhao, W.-F. Dong and W. Liu, *ACS Nano*, 2017, **11**, 3496–3505.
- J.-M. Lim, N. Bertrand, P. M. Valencia, M. Rhee, R. Langer, S. Jon, O. C. Farokhzad and R. Karnik, *Nanomedicine*, 2014, **10**, 401–409.
- D. M. Headen, J. R. García and A. J. García, *Microsyst. Nanoeng.*, 2018, **4**, 17076.
- A. Khurana, P. Allawadhi, I. Khurana, S. Allwadhi, R. Weiskirchen, A. K. Banothu, D. Chhabra, K. Joshi and K. K. Bharani, *Nano Today*, 2021, **38**, 101142.
- M. Maeki, S. Uno, A. Niwa, Y. Okada and M. Tokeshi, *J. Controlled Release*, 2022, **344**, 80–96.
- F. P. Polack, S. J. Thomas, N. Kitchin, J. Absalon, A. Gurtman, S. Lockhart, J. L. Perez, G. Pérez Marc, E. D. Moreira, C. Zerbini, R. Bailey, K. A. Swanson, S. Roychoudhury, K. Koury, P. Li, W. V. Kalina, D. Cooper, R. W. Frenck, L. L. Hammitt, Ö. Türeci, H. Nell, A. Schaefer, S. Ünal, D. B. Tresnan, S. Mather, P. R. Dormitzer, U. Şahin, K. U. Jansen and W. C. Gruber, *N. Engl. J. Med.*, 2020, **383**, 2603–2615.
- K. Osouli-Bostanabad, S. Puliga, D. R. Serrano, A. Bucchi, G. Halbert and A. Lalatsa, *Pharmaceutics*, 2022, **14**, 1940.
- R. Tenchov, R. Bird, A. E. Curtze and Q. Zhou, *ACS Nano*, 2021, **15**, 16982–17015.
- F. Aldeek, M. Safi, N. Zhan, G. Palui and H. Mattoussi, *ACS Nano*, 2013, **7**, 10197–10210.
- M. Cao, R. Xing, R. Chang, Y. Wang and X. Yan, *Coord. Chem. Rev.*, 2019, **397**, 14–27.
- B. Bednář, K. Edwards, M. Almgren, S. Tormod and Z. Tuzar, *Die Makromolekulare Chemie, Rapid Communications*, 1988, **9**, 785–790.
- J. Cravillon, C. A. Schröder, R. Nayuk, J. Gummel, K. Huber and M. Wiebcke, *Angew. Chem., Int. Ed.*, 2011, **50**, 8067–8071.
- P. M. Valencia, O. C. Farokhzad, R. Karnik and R. Langer, *Nat. Nanotechnol.*, 2012, **7**, 623–629.
- O. Söhnle and J. W. Mullin, *J. Colloid Interface Sci.*, 1988, **123**, 43–50.
- D. Liu, S. Cito, Y. Zhang, C. F. Wang, T. M. Sikanen and H. A. Santos, *Adv. Mater.*, 2015, **27**, 2298–2304.

- 42 S. J. Shepherd, C. C. Warzecha, S. Yadavali, R. El-Mayta, M.-G. Alameh, L. Wang, D. Weissman, J. M. Wilson, D. Issadore and M. J. Mitchell, *Nano Lett.*, 2021, **21**, 5671–5680.
- 43 M. Maeki, Y. Okada, S. Uno, K. Sugiura, Y. Suzuki, K. Okuda, Y. Sato, M. Ando, H. Yamazaki, M. Takeuchi, A. Ishida, H. Tani, H. Harashima and M. Tokeshi, *Appl. Mater. Today*, 2023, **31**, 101754.
- 44 W. Zhang, A. Mehta, Z. Tong, L. Esser and N. H. Voelcker, *Adv. Sci.*, 2021, **8**, 2003937.
- 45 A. Zinger, M. Sushnitha, T. Naoi, G. Baudo, E. De Rosa, J. Chang, E. Tasciotti and F. Taraballi, *ACS Nano*, 2021, **15**, 6326–6339.
- 46 F. S. Majedi, M. M. Hasani-Sadrabadi, J. J. VanDersarl, N. Mokarram, S. Hojjati-Emami, E. Dashtimoghadam, S. Bonakdar, M. A. Shokrgozar, A. Bertsch and P. Renaud, *Adv. Funct. Mater.*, 2014, **24**, 432–441.
- 47 A. Albanese, P. S. Tang and W. C. Chan, *Annu. Rev. Biomed. Eng.*, 2012, **14**, 1–16.
- 48 N. Hoshyar, S. Gray, H. Han and G. Bao, *Nanomedicine*, 2016, **11**, 673–692.
- 49 A. J. Mieszawska, Y. Kim, A. Gianella, I. van Rooy, B. Priem, M. P. Labarre, C. Ozcan, D. P. Cormode, A. Petrov and R. Langer, *Bioconjugate Chem.*, 2013, **24**, 1429–1434.
- 50 M. M. Hasani-Sadrabadi, V. Karimkhani, F. S. Majedi, J. J. Van Dersarl, E. Dashtimoghadam, F. Afshar-Taromi, H. Mirzadeh, A. Bertsch, K. I. Jacob and P. Renaud, *Adv. Mater.*, 2014, **26**, 3118–3123.
- 51 R. Karnik, F. Gu, P. Basto, C. Cannizzaro, L. Dean, W. Kyei-Manu, R. Langer and O. C. Farokhzad, *Nano Lett.*, 2008, **8**, 2906–2912.
- 52 B. T. Luk and L. Zhang, *J. Controlled Release*, 2015, **220**, 600–607.
- 53 T. Yong, X. Zhang, N. Bie, H. Zhang, X. Zhang, F. Li, A. Hakeem, J. Hu, L. Gan, H. A. Santos and X. Yang, *Nat. Commun.*, 2019, **10**, 3838.
- 54 P. Fathi, L. Rao and X. Chen, *View*, 2020, **2**, 20200187.
- 55 A. D. Stroock, S. K. W. Dertinger, A. Ajdari, I. Mezić, H. A. Stone and G. M. Whitesides, *Science*, 2002, **295**, 647–651.
- 56 A. Jahn, S. M. Stavis, J. S. Hong, W. N. Vreeland, D. L. DeVoe and M. Gaitan, *ACS Nano*, 2010, **4**, 2077–2087.
- 57 R. F. Pagels, J. Edelstein, C. Tang and R. K. Prud'homme, *Nano Lett.*, 2018, **18**, 1139–1144.
- 58 B. K. Johnson and R. K. Prud'homme, *Phys. Rev. Lett.*, 2003, **91**, 118302.
- 59 N. M. Belliveau, J. Huft, P. J. C. Lin, S. Chen, A. K. K. Leung, T. J. Leaver, A. W. Wild, J. B. Lee, R. J. Taylor, Y. K. Tam, C. L. Hansen and P. R. Cullis, *Mol. Ther.–Nucleic Acids*, 2012, **1**, e37.
- 60 C.-C. Hong, J.-W. Choi and C. H. Ahn, *Lab Chip*, 2004, **4**, 109–113.
- 61 S. Hossain, M. A. Ansari, A. Husain and K.-Y. Kim, *Chem. Eng. J.*, 2010, **158**, 305–314.
- 62 J. Li, G. Xia and Y. Li, *J. Chem. Technol. Biotechnol.*, 2013, **88**, 1757–1765.
- 63 T. M. Squires and S. R. Quake, *Rev. Mod. Phys.*, 2005, **77**, 977–1026.
- 64 J. Sun, Y. Xianyu, M. Li, W. Liu, L. Zhang, D. Liu, C. Liu, G. Hu and X. Jiang, *Nanoscale*, 2013, **5**, 5262–5265.
- 65 J. Wang, W. Chen, J. Sun, C. Liu, Q. Yin, L. Zhang, Y. Xianyu, X. Shi, G. Hu and X. Jiang, *Lab Chip*, 2014, **14**, 1673–1677.
- 66 Y. Kim, B. Lee Chung, M. Ma, W. J. M. Mulder, Z. A. Fayad, O. C. Farokhzad and R. Langer, *Nano Lett.*, 2012, **12**, 3587–3591.
- 67 M. Gonidec and J. Puigmartí-Luis, *Crystals*, 2018, **9**, 12.
- 68 D. J. Collins, A. Neild, A. deMello, A. Q. Liu and Y. Ai, *Lab Chip*, 2015, **15**, 3439–3459.
- 69 X. Jiang, S. Li, K.-I. Sotowa, O. Tonomura and T. Hoon Oh, *Chem. Eng. J.*, 2023, **471**, 144546.
- 70 S. Abalde-Cela, P. Taladriz-Blanco, M. G. de Oliveira and C. Abell, *Sci. Rep.*, 2018, **8**, 2440.
- 71 K. S. Huang, C. H. Yang, Y. C. Wang, W. T. Wang and Y. Y. Lu, *Pharmaceutics*, 2019, **11**, 212.
- 72 I. Lignos, S. Stavrikis, G. Nedelcu, L. Protesescu, A. J. deMello and M. V. Kovalenko, *Nano Lett.*, 2016, **16**, 1869–1877.
- 73 L. Amirifar, M. Besanjideh, R. Nasiri, A. Shamloo, F. Nasrollahi, N. R. de Barros, E. Davoodi, A. Erdem, M. Mahmoodi, V. Hosseini, H. Montazerian, J. Jahangiry, M. A. Darabi, R. Haghniaz, M. R. Dokmeci, N. Annabi, S. Ahadian and A. Khademhosseini, *Biofabrication*, 2022, **14**, 022001.
- 74 S. Sohrabi, N. Kassir and M. Keshavarz Moraveji, *RSC Adv.*, 2020, **10**, 27560–27574.
- 75 Z. Chen, S. Kheiri, E. W. K. Young and E. Kumacheva, *Langmuir*, 2022, **38**, 6233–6248.
- 76 J. N. Belling, L. K. Heidenreich, Z. Tian, A. M. Mendoza, T.-T. Chiou, Y. Gong, N. Y. Chen, T. D. Young, N. Wattanatorn, J. H. Park, L. Scarabelli, N. Chiang, J. Takahashi, S. G. Young, A. Z. Stieg, S. De Oliveira, T. J. Huang, P. S. Weiss and S. J. Jonas, *Proc. Natl. Acad. Sci. U. S. A.*, 2020, **117**, 10976–10982.
- 77 I. Lentacker, I. De Cock, R. Deckers, S. C. De Smedt and C. T. W. Moonen, *Adv. Drug Delivery Rev.*, 2014, **72**, 49–64.
- 78 F. Mahmud, K. F. Tamrin, S. Mohamaddan and N. Watanabe, *Processes*, 2021, **9**, 891.
- 79 V. Sebastián and K. F. Jensen, *Nanoscale*, 2016, **8**, 15288–15295.
- 80 K. O. Rojek, M. Ćwiklińska, J. Kuczak and J. Guzowski, *Chem. Rev.*, 2022, **122**, 16839–16909.
- 81 D.-Y. Kim, S. H. Jin, S.-G. Jeong, B. Lee, K.-K. Kang and C.-S. Lee, *Sci. Rep.*, 2018, **8**, 8525.
- 82 T. Kotnik, L. Rems, M. Tarek and D. Miklavčič, *Ann. Rev. Biophys.*, 2019, **48**, 63–91.
- 83 L. Lin, J. Zhang, X. Peng, Z. Wu, A. C. H. Coughlan, Z. Mao, M. A. Bevan and Y. Zheng, *Sci. Adv.*, 2017, **3**, e1700458.
- 84 L. Schoenmaker, D. Witzigmann, J. A. Kulkarni, R. Verbeke, G. Kersten, W. Jiskoot and D. J. A. Crommelin, *Int. J. Pharm.*, 2021, **601**, 120586.
- 85 M. J. Ostro, D. Giacomoni, D. O. N. Lavelle, W. Paxton and S. Dray, *Nature*, 1978, **274**, 921–923.
- 86 G. J. Dimitriadis, *Nature*, 1978, **274**, 923–924.
- 87 P. L. Felgner, T. R. Gadek, M. Holm, R. Roman, H. W. Chan, M. Wenz, J. P. Northrop, G. M. Ringold and



- M. Danielsen, *Proc. Natl. Acad. Sci. U. S. A.*, 1987, **84**, 7413–7417.
- 88 A. L. Bailey and P. R. Cullis, *Biochemistry*, 1994, **33**, 12573–12580.
- 89 A. A. Barba, S. Bochicchio, A. Dalmoro and G. Lamberti, *Pharmaceutics*, 2019, **11**, 360.
- 90 Y. Li, R. J. Lee, X. Huang, Y. Li, B. Lv, T. Wang, Y. Qi, F. Hao, J. Lu, Q. Meng, L. Teng, Y. Zhou, J. Xie and L. Teng, *Nanomedicine*, 2017, **13**, 371–381.
- 91 M. J. W. Evers, J. A. Kulkarni, R. van der Meel, P. R. Cullis, P. Vader and R. M. Schiffelers, *Small Methods*, 2018, **2**, 1700375.
- 92 L. B. Jeffs, L. R. Palmer, E. G. Ambegia, C. Giesbrecht, S. Ewanick and I. MacLachlan, *Pharm. Res.*, 2005, **22**, 362–372.
- 93 T. S. Zimmermann, A. C. H. Lee, A. Akinc, B. Bramlage, D. Bumcrot, M. N. Fedoruk, J. Harborth, J. A. Heyes, L. B. Jeffs, M. John, A. D. Judge, K. Lam, K. McClintock, L. V. Nechev, L. R. Palmer, T. Racie, I. Röhl, S. Seiffert, S. Shanmugam, V. Sood, J. Soutschek, I. Toudjarska, A. J. Wheat, E. Yaworski, W. Zedalis, V. Koteliensky, M. Manoharan, H.-P. Vornlocher and I. MacLachlan, *Nature*, 2006, **441**, 111–114.
- 94 A. Jahn, W. N. Vreeland, M. Gaitan and L. E. Locascio, *J. Am. Chem. Soc.*, 2004, **126**, 2674–2675.
- 95 D. Chen, K. T. Love, Y. Chen, A. A. Eltoukhy, C. Kastrup, G. Sahay, A. Jeon, Y. Dong, K. A. Whitehead and D. G. Anderson, *J. Am. Chem. Soc.*, 2012, **134**, 6948–6951.
- 96 M. A. Younis, I. A. Khalil, Y. H. A. Elewa, Y. Kon and H. Harashima, *J. Controlled Release*, 2021, **331**, 335–349.
- 97 S. Ramishetti, R. Kedmi, M. Goldsmith, F. Leonard, A. G. Sprague, B. Godin, M. Gozin, P. R. Cullis, D. M. Dykxhoorn and D. Peer, *ACS Nano*, 2015, **9**, 6706–6716.
- 98 C. Jiang, M. Mei, B. Li, X. Zhu, W. Zu, Y. Tian, Q. Wang, Y. Guo, Y. Dong and X. Tan, *Cell Res.*, 2017, **27**, 440–443.
- 99 D. Rosenblum, A. Gutkin, R. Kedmi, S. Ramishetti, N. Veiga, A. M. Jacobi, M. S. Schubert, D. Friedmann-Morvinski, Z. R. Cohen, M. A. Behlke, J. Lieberman and D. Peer, *Sci. Adv.*, 2020, **6**, eabc9450.
- 100 M. Rhee, P. M. Valencia, M. I. Rodriguez, R. Langer, O. C. Farokhzad and R. Karnik, *Adv. Mater.*, 2011, **23**, H79–H83.
- 101 M. H. M. Leung and A. Q. Shen, *Langmuir*, 2018, **34**, 3961–3970.
- 102 D. J. Hines and D. L. Kaplan, *Crit. Rev. Ther. Drug Carrier Syst.*, 2013, **30**, 257–276.
- 103 Q. Feng, J. Liu, X. Li, Q. Chen, J. Sun, X. Shi, B. Ding, H. Yu, Y. Li and X. Jiang, *Small*, 2017, **13**, 1603109.
- 104 N. Anton, F. Bally, C. A. Serra, A. Ali, Y. Arntz, Y. Mely, M. Zhao, E. Marchioni, A. Jakhmola and T. F. Vandamme, *Soft Matter*, 2012, **8**, 10628–10635.
- 105 E. Jafarifar, M. Hajialyani, M. Akbari, M. Rahimi, Y. Shokohinia and A. Fattahi, *Pharm. Dev. Technol.*, 2017, **22**, 836–843.
- 106 L. Chronopoulou, C. Sparago and C. Palocci, *J. Nanopart. Res.*, 2014, **16**, 2703.
- 107 Q. Xu, M. Hashimoto, T. T. Dang, T. Hoare, D. S. Kohane, G. M. Whitesides, R. Langer and D. G. Anderson, *Small*, 2009, **5**, 1575–1581.
- 108 N. Kolishetti, S. Dhar, P. M. Valencia, L. Q. Lin, R. Karnik, S. J. Lippard, R. Langer and O. C. Farokhzad, *Proc. Natl. Acad. Sci. U. S. A.*, 2010, **107**, 17939–17944.
- 109 E. Chiesa, A. Greco, F. Riva, E. M. Tosca, R. Dorati, S. Pisani, T. Modena, B. Conti and I. Genta, *Int. J. Mol. Sci.*, 2019, **20**, 6212.
- 110 N. Escareño, N. Hassan, M. J. Kogan, J. Juárez, A. Topete and A. Daneri-Navarro, *J. Colloid Interface Sci.*, 2021, **591**, 440–450.
- 111 M. Russo, P. Bevilacqua, P. A. Netti and E. Torino, *Sci. Rep.*, 2016, **6**, 37906.
- 112 T. H. Tran, C. T. Nguyen, D.-P. Kim, Y.-K. Lee and K. M. Huh, *Lab Chip*, 2012, **12**, 589–594.
- 113 Z. Mahmoudi, J. Mohammadnejad, S. Razavi Bazaz, A. Abouei Mehrizi, M. Saidijam, R. Dinarvand, M. Ebrahimi Warkiani and M. Soleimani, *Carbohydr. Polym.*, 2020, **229**, 115551.
- 114 B. Wu, C. Yang, B. Li, L. Feng, M. Hai, C.-X. Zhao, D. Chen, K. Liu and D. A. Weitz, *Small*, 2020, **16**, 2002716.
- 115 Y. Zhang, J. Feng, S. A. McManus, H. D. Lu, K. D. Ristorph, E. J. Cho, E. L. Dobrijevic, H.-K. Chan and R. K. Prud'homme, *Mol. Pharm.*, 2017, **14**, 3480–3488.
- 116 N. Lababidi, V. Sigal, A. Koenneke, K. Schwarzkopf, A. Manz and M. Schneider, *Beilstein J. Nanotechnol.*, 2019, **10**, 2280–2293.
- 117 W. Zhang, J. Li, C. P. Silveira, Q. Cai, K. A. Dawson, G. Cagney and Y. Yan, *PNAS Nexus*, 2022, **1**, pgac172.
- 118 W. Zhang, H. Lopez, L. Boselli, P. Bigini, A. Perez-Potti, Z. Xie, V. Castagnola, Q. Cai, C. P. Silveira, J. M. de Araujo, L. Talamini, N. Panini, G. Ristagno, M. B. Violatto, S. Devineau, M. P. Monopoli, M. Salmona, V. A. Giannone, S. Lara, K. A. Dawson and Y. Yan, *ACS Nano*, 2022, **16**, 1547–1559.
- 119 L. Boselli, H. Lopez, W. Zhang, Q. Cai, V. A. Giannone, J. Li, A. Moura, J. M. de Araujo, J. Cookman, V. Castagnola, Y. Yan and K. A. Dawson, *Commun. Mater.*, 2020, **1**, 35.
- 120 P. M. Valencia, E. M. Pridgen, M. Rhee, R. Langer, O. C. Farokhzad and R. Karnik, *ACS Nano*, 2013, **7**, 10671–10680.
- 121 D. Liu, H. Zhang, S. Cito, J. Fan, E. Mäkilä, J. Salonen, J. Hirvonen, T. M. Sikanen, D. A. Weitz and H. A. Santos, *Nano Lett.*, 2017, **17**, 606–614.
- 122 L. Zhang, Q. Feng, J. Wang, J. Sun, X. Shi and X. Jiang, *Angew. Chem., Int. Ed.*, 2015, **54**, 3952–3956.
- 123 D. L. Fang, Y. Chen, B. Xu, K. Ren, Z. Y. He, L. L. He, Y. Lei, C. M. Fan and X. R. Song, *Int. J. Mol. Sci.*, 2014, **15**, 3373–3388.
- 124 H. Furukawa, K. E. Cordova, M. O'Keeffe and O. M. Yaghi, *Science*, 2013, **341**, 1230444.
- 125 G. Cheng, W. Li, L. Ha, X. Han, S. Hao, Y. Wan, Z. Wang, F. Dong, X. Zou, Y. Mao and S.-Y. Zheng, *J. Am. Chem. Soc.*, 2018, **140**, 7282–7291.
- 126 Y. L. Balachandran, X. Li and X. Jiang, *Nano Lett.*, 2021, **21**, 1335–1344.
- 127 C. Hu, Y. Bai, M. Hou, Y. Wang, L. Wang, X. Cao, C.-W. Chan, H. Sun, W. Li, J. Ge and K. Ren, *Sci. Adv.*, 2020, **6**, eaax5785.
- 128 S. Sevim, A. Sorrenti, J. P. Vale, Z. El-Hachemi, S. Pané, A. D. Flouris, T. S. Mayor and J. Puigmartí-Luis, *Nat. Commun.*, 2022, **13**, 1766.

- 129 B. A. Grzybowski, Y. I. Sobolev, O. Cybulski and B. Mikulak-Klucznik, *Nat. Rev. Mater.*, 2022, 7, 338–354.
- 130 Y. Li, C. Liu, X. Bai, F. Tian, G. Hu and J. Sun, *Angew. Chem., Int. Ed.*, 2020, 59, 3486–3490.
- 131 W. Lv, Z. Han, Y. Li, Y. Huang, J. Sun, X. Lu and C. Liu, *Chin. J. Chem.*, 2021, 39, 2107–2112.
- 132 S.-Y. Tang, R. Qiao, S. Yan, D. Yuan, Q. Zhao, G. Yun, T. P. Davis and W. Li, *Small*, 2018, 14, 1800118.
- 133 N. H. An, Le, H. Deng, C. Devendran, N. Akhtar, X. Ma, C. Pouton, H.-K. Chan, A. Neild and T. Alan, *Lab Chip*, 2020, 20, 582–591.
- 134 A. Pourabed, T. Younas, C. Liu, B. K. Shanbhag, L. He and T. Alan, *J. Colloid Interface Sci.*, 2021, 585, 229–236.
- 135 M. Kim, J.-H. Lee and J.-M. Nam, *Adv. Sci.*, 2019, 6, 1900471.
- 136 G.-X. Li, Q. Li, R. Cheng and S. Chen, *Curr. Opin. Chem. Eng.*, 2020, 29, 34–41.
- 137 Z. Zhu, Z. Guan, S. Jia, Z. Lei, S. Lin, H. Zhang, Y. Ma, Z.-Q. Tian and C. J. Yang, *Angew. Chem., Int. Ed.*, 2014, 53, 12503–12507.
- 138 X. Li, M. Zha, Y. Li, J.-S. Ni, T. Min, T. Kang, G. Yang, H. Tang, K. Li and X. Jiang, *Angew. Chem., Int. Ed.*, 2020, 59, 21899–21903.
- 139 Z. Liu, W. Lian, Q. Long, R. Cheng, G. Torrieri, B. Zhang, A. Koivuniemi, M. Mahmoudzadeh, A. Bunker, H. Gao, H. He, Y. Chen, J. Hirvonen, R. Zhou, Q. Zhao, X. Ye, X. Deng and H. A. Santos, *Adv. Funct. Mater.*, 2022, 32, 2204666.
- 140 J. Mahin and L. Torrente-Murciano, *Chem. Eng. J.*, 2020, 396, 125299.
- 141 Z.-H. Tian, Y.-J. Wang, J.-H. Xu and G.-S. Luo, *Chem. Eng. J.*, 2016, 302, 498–502.
- 142 Y. Shu, P. Jiang, D.-W. Pang and Z.-L. Zhang, *Nanotechnology*, 2015, 26, 275701.
- 143 A. M. Nightingale, S. H. Krishnadasan, D. Berhanu, X. Niu, C. Drury, R. McIntyre, E. Valsami-Jones and J. C. deMello, *Lab Chip*, 2011, 11, 1221–1227.
- 144 S. Tian, M. Fu, W. Hoheisel and L. Mleczko, *Chem. Eng. J.*, 2016, 289, 365–373.
- 145 J. Baek, Y. Shen, I. Lignos, M. G. Bawendi and K. F. Jensen, *Angew. Chem., Int. Ed.*, 2018, 57, 10915–10918.
- 146 L. Lin, M. Wang, X. Peng, E. N. Lissek, Z. Mao, L. Scarabelli, E. Adkins, S. Coskun, H. E. Unalan, B. A. Korgel, L. M. Liz-Marzán, E.-L. Florin and Y. Zheng, *Nat. Photonics*, 2018, 12, 195–201.
- 147 J. Li and Y. Zheng, *Acc. Mater. Res.*, 2021, 2, 352–363.
- 148 A. M. Mebert, C. Aimé, G. S. Alvarez, Y. Shi, S. A. Flor, S. E. Lucangioli, M. F. Desimone and T. Coradin, *J. Mater. Chem. B*, 2016, 4, 3135–3144.
- 149 D. Kalyane, N. Kumar, N. Anup, K. Rajpoot, R. Maheshwari, P. Sengupta, K. Kalia and R. K. Tekade, *Int. J. Pharm.*, 2021, 609, 121173.
- 150 C. Y. Li, K. R. Stevens, R. E. Schwartz, B. S. Alejandro, J. H. Huang and S. N. Bhatia, *Tissue Eng., Part A*, 2014, 20, 2200–2212.
- 151 H. Wang, H. Liu, H. Liu, W. Su, W. Chen and J. Qin, *Adv. Mater. Technol.*, 2019, 4, 1800632.
- 152 K. S. Paulsen, D. Di Carlo and A. J. Chung, *Nat. Commun.*, 2015, 6, 6976.
- 153 K. S. Paulsen, Y. Deng and A. J. Chung, *Adv. Sci.*, 2018, 5, 1800252.
- 154 P. Perez Schmidt, K. Pagano, C. Lenardi, M. Penconi, R. M. Ferrando, C. Evangelisti, L. Lay, L. Ragona, M. Marelli and L. Polito, *Angew. Chem., Int. Ed.*, 2023, 62, e202210140.
- 155 R. Mateu Ferrando, L. Lay and L. Polito, *Drug Discovery Today*, 2020, 38, 57–67.
- 156 M. Anderluh, F. Berti, A. Bzducha-Wróbel, F. Chiodo, C. Colombo, F. Compostella, K. Durlík, X. Ferhati, R. Holmdahl, D. Jovanovic, W. Kaca, L. Lay, M. Marinovic-Cincovic, M. Marradi, M. Ozil, L. Polito, J. J. Reina, C. A. Reis, R. Sackstein, A. Silipo, U. Švajger, O. Vaněk, F. Yamamoto, B. Richichi and S. J. van Vliet, *FEBS J.*, 2022, 289, 4251–4303.
- 157 D. Ferraro, Y. Lin, B. Teste, D. Talbot, L. Malaquin, S. Descroix and A. Abou-Hassan, *Chem. Commun.*, 2015, 51, 16904–16907.